

THESIS

CHARACTERIZATION OF INTERACTIONS OF LIPOQUINONE DERIVATIVES
WITHIN MODEL MEMBRANE SYSTEMS

Submitted by

Gaia Rachel Bublitz

Department of Biochemistry & Molecular Biology

In partial fulfillment of the requirements

For the Degree of Master of Science

Colorado State University

Fort Collins, Colorado

Summer 2021

Master's Committee:

Advisor: Robert Cohen
Co-Advisor: Debbie Crans

Thomas Santangelo
Deborah Roess

Copyright by Gaia Rachel Bublitz 2021

All Rights Reserved

ABSTRACT

CHARACTERIZATION OF INTERACTIONS OF LIPOQUINONE DERIVATIVES WITHIN MODEL MEMBRANE SYSTEMS

Menaquinones (MK) are electron carriers composed of a naphthoquinone moiety and an isoprene side chain of variable length and saturation. These molecules are the only quinone derivatives present in the electron transport systems of all Gram-positive bacteria and some Gram-negative anaerobes. Subsequently, MK plays a critical role in respiration for pathogens such as *Staphylococcus aureus* and *Mycobacterium tuberculosis*. Although the physiological function and relevance of MK as a redox cofactor have been established, its chemical interactions within the plasma membrane and the effects of these properties on MK-mediated electron transport are still obscure. These unknowns are reflected in existing literature, as MK is commonly depicted in an extended conformation, although *in vitro* and *in vivo* studies suggest that biomolecules with alkyl moieties assume folded conformations in native environments (Ko et al., 2011; Trembleau et al., 2003). In this study, we implemented 1D ^1H and 2D ^1H - ^1H NMR spectroscopic techniques to characterize the location and 3D conformation of MK-2 within a L- α -phosphatidylcholine liposome model. MK-2, a truncated menaquinone analog, was selected due to its limited rotational variability and previous characterization in a simple monolayer lipid system (Koehn et al., 2018). Our data suggests that MK-2 is largely incorporated into the phospholipid bilayer, with an aqueous subspecies residing at the polar membrane interface in a concentration-

dependent manner. 2D NOESY spectroscopic analysis supports the interpretation that both the aqueous form and the membrane-associated form of MK-2 assume a folded conformation. These findings provide a reference for the study of the properties of MK derivatives with longer isoprene chains, which are analogous to functional MK variants in native environments.

TABLE OF CONTENTS

ABSTRACT	ii
Chapter 1 - Introduction.....	1
1.1 Menaquinone (MK) Activity in Biological Systems.....	1
1.1.1 Menaquinone Function in the Prokaryotic Electron Transport Chain.....	2
1.1.2 Menaquinone Biosynthesis	3
1.1.3 Menaquinone-Associating Proteins as Antimicrobial Targets	6
1.1.4 Menaquinone Catalytic Mechanism.....	6
1.1.5 Role of the Isoprene Chain in Menaquinone Function	8
1.1.6 Conformation of Quinone Derivatives in Cell Membranes	9
1.2 Studies of Menaquinone Properties in Model Membranes.....	10
Chapter 2: Utilization of Model Membranes and NMR Spectroscopy for Biologically Relevant Research.....	13
2.1 Membrane Mimetics Used to Model Biological Membranes.....	13
2.1.1 Solvents and Self-Assembled Structures Used as Model Membranes.....	13
2.1.2 Liposome Preparation Techniques.....	15
2.1.3 Biological Considerations for Liposome Preparation & Formulation	16
2.1.4 Applications of NMR Spectroscopy to Studies of Liposomal Systems.....	17
Chapter 3 – Materials & Methods.....	21
3.1 Method Development.....	21
3.1.1 Optimization of Liposome Preparation and Incorporation of MK-2	21
3.1.2 Liposome Sample Stability	22
3.1.3 Comparison of MK-2 Derivatives for NMR Spectroscopic Studies	24
3.2 Procedures.....	26

3.2.1 General.....	26
3.2.2 Preparation of Liposomes Incorporated with MK-2 for NMR Spectroscopic Studies	26
3.2.3 Preparation of Liposomes incorporated with MK-2 for Dynamic Light Scattering Analysis (DLS)	26
3.2.4 NMR Spectroscopic Studies	27
3.2.5 1D ^1H and 2D ^1H - ^1H NMR Studies of MK-2 in Liposomes.....	27
3.2.6 1D ^1H T_1 Relaxation Experiments	28
3.2.7 DLS Studies.....	28
3.2.8 Molecular Mechanics Analysis	28
3.2.9 Statistical Analysis.....	28
Chapter 4 – Results & Discussion.....	30
4.1 1D ^1H NMR Spectroscopic Analysis of MK-2 in Liposome Vesicles.....	30
4.2 2D ^1H - ^1H NMR Spectroscopic Analysis of MK-2 in Liposome Vesicles	35
4.3 ^1H - ^1H NOESY NMR of Liposomes Incorporating 19 mM MK-2.....	36
4.4 ^1H - ^1H NOESY NMR of Liposomes Incorporating 39 mM MK-2.....	40
4.5 ^1H - ^1H NOESY NMR of Liposomes Incorporating 36 mM MK-2.....	43
4.6 ^1H - ^1H 2D NOESY NMR of 39 mM MK-2 in Aqueous Solvent.....	43
4.7 Inversion Recovery ^1H NMR Spectroscopic Experiments	45
4.8 Molecular Mechanics Simulations.....	48
Chapter 5 – Conclusions.....	50
References.....	57
Appendices	70

Chapter 1 - Introduction

1.1 Menaquinone (MK) Activity in Biological Systems: Quinones are believed to be one of the oldest groups of organic molecules in the universe (Krueger et al., 2004), and isoprenoid quinones in particular are integral for energy metabolism in a multitude of biological organisms. Menaquinones (MK) are the oldest and most widely conserved lipoquinone derivatives across the phylogenetic tree, transporting electrons between membrane protein complexes in the respiratory chains of many facultative and obligate anaerobes, and some species of archaea (Nowicka et al., 2010, Upadhyay et al., 2015). These membrane-bound MK molecules are composed of a naphthoquinone moiety and an isoprenoid chain that is typically composed of 6-10 isoprenyl units, although derivatives containing 1-14 isoprenyl units have also been observed (Nowicka et al., 2010).

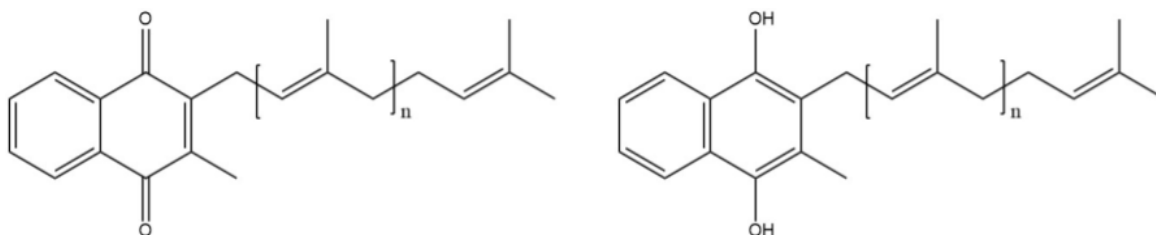


Figure 1: The general structure of menaquinone (MK) and its reduced menaquinol form (MKH₂). Length n of the isoprenyl chain varies across species. Figure created using ChemDraw Professional 16.0.

Since MK is the sole quinone variant for pathogens such as *M. tuberculosis* and *S. aureus* (Choi et al., 2017; Lu et al., 2008) and is absent in mammalian respiratory pathways (Boersch et al., 2018), enzymes in the MK biosynthetic pathway and MK-associated proteins are being investigated as targets for reducing pathogen virulence

and addressing pharmacological challenges related to antimicrobial resistance. MK itself is a potential drug target; Lycosin E has been identified as an antibiotic with a novel mode of action that binds directly to MK and is believed to disrupt the microbial membrane potential (Paudel et al., 2016). Recent studies suggest that the susceptibility of different *S. aureus* strains to Lycosin E may be dependent on MK isoprene chain length variability (Panthee et al., 2020). However, the manner in which structural variability of MK analogs influences MK interactions with both respiratory chain proteins and the bulk membrane is not well understood, hindering drug discovery targeting MK and MK-utilizing proteins.

Information regarding the molecular dynamics and enzyme kinetics of MK is limited by challenges in measuring the activity of membrane-associated proteins and molecules, which require the hydrophobic environment of the cell membrane for proper function. Conducting assays to measure MK enzymatic activity is complicated by the insolubility of native MK molecules in aqueous solution due to their long alkyl chains (Upadhyay et al., 2018). Subsequently, our laboratory utilizes truncated MK derivatives to elucidate information regarding MK conformation and interactions within model membranes. By obtaining fundamental information regarding MK interactions within simplified systems, our objective is to use laboratory experiments to support *in vitro* and *in silico* projects investigating the relationship between MK structure, conformation, and catalytic activity.

1.1.1 Menaquinone Function in the Prokaryotic Electron Transport Chain: The microbial electron transport chain (ETC) is comprised of a succession of membrane-bound protein complexes that mediate electron transfer (Thompson et al., 2019). In the ETC of MK-utilizing microbes, MK molecules diffuse across the plasma membrane,

transferring electrons between ETC enzymes (Kurosu et al., 2010; Upadhyay et al., 2015). This exchange of electrons is paired with proton transfer, resulting in the transient conversion of MK between its oxidized and reduced (MKH₂) forms (Boersch et al., 2018; Nowicka et al., 2010; Upadhyay et al., 2015). The electron transfer process is essential for the perpetuation of a proton motive force across the membrane, which produces an electrochemical gradient that is essential for the oxidative phosphorylation of ADP by ATP synthase (Grimaldi et al., 2012; Thompson et al., 2019; Yano et al., 2014). The energy conversion efficiency of this process is dependent on both 1) the binding kinetics of MK, and 2) the diffusion rate of MK between transmembrane complexes (Singharoy et al., 2019; Yano et al., 2014). The structure and conformation of MK derivatives, as well as the composition of the native membrane itself, are key determinants of these factors.

1.1.2 Menaquinone Biosynthesis: Current findings indicate that microbial species synthesize MK via one of two pathways, referred to as the “classical” pathway and the

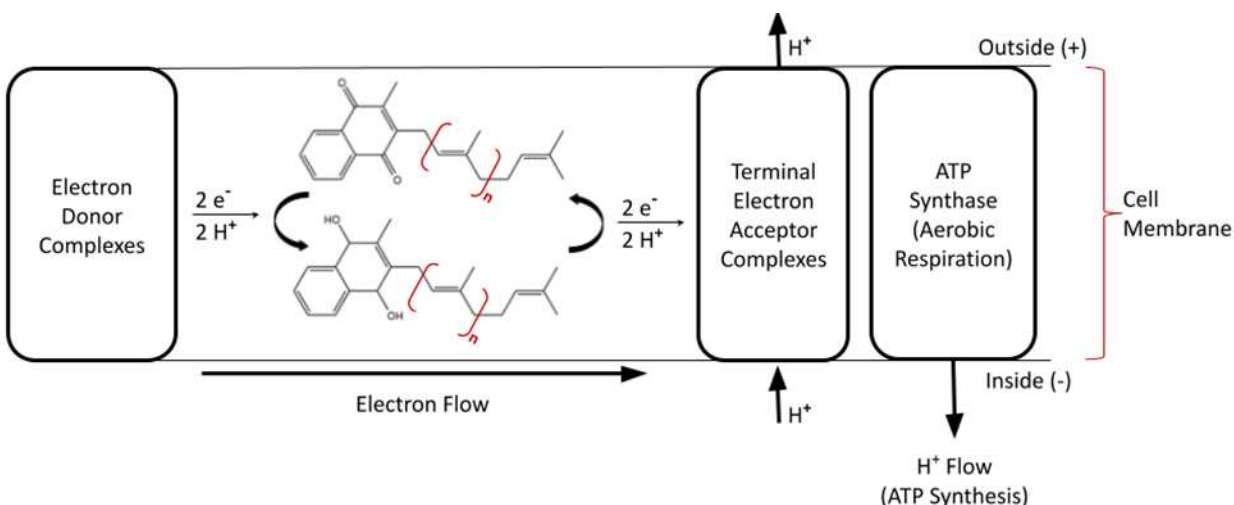


Figure 2: General schematic of the bacterial electron transport system. Figure is derived and updated with significant modifications from a figure by Upadhyay et al., 2015.

recently identified “futasoline” pathway (Hiratsuka et al., 2008; Johnston & Bulloch 2020; Joshi et al., 2018). The classical biosynthetic mechanism is utilized by pathogens such as *M. tuberculosis* and *S. aureus* (Bashiri et al., 2020; Hiratsuka et al., 2008; Panthee et al., 2020). In the first steps of the classical pathway, the naphthoquinone head group and isoprene chain are synthesized separately in the cytosol (Johnston & Bulloch 2020). Synthesis of a naphthoate precursor to the naphthoquinone head group of MK is catalyzed by a series of enzymes (Figure 3), resulting in the conversion of chorismate to 1,4-dihydroxy-2-naphthoic acid (DHNA) (Bashiri et al., 2020; Boersch et al., 2018; Johnston & Bulloch, 2020). Synthesis of the isoprene chain is catalyzed by variants of the isoprenyl diphosphate synthase family (Johnston & Bulloch 2020).

The subsequent steps of MK biosynthesis are catalyzed by membrane-bound enzymes (Johnston & Bulloch 2020). A transmembrane prenyltransferase known as MenA replaces the carboxylate group on DHNA with the nascent isoprene chain (Johnston & Bulloch 2020), lending lipid-soluble properties to the MK precursor molecule.

Methylation of the naphthoquinone moiety is conducted by MenG methyltransferase to produce the final MK product (Zhang et al., 2021). In some organisms, downstream enzymes introduce additional modifications to MK derivatives. MenJ, a membrane-bound reductase which has been found in mycobacteria, saturates the β -isoprene unit of MK-9 (Puffal et al., 2018; Upadhyay et al., 2015, 2018). While the cytosolic enzymes involved in MK biosynthesis have been well-characterized, the structures of membrane-associating MK biosynthetic enzymes in the later steps of the pathway are still obscure (Johnston & Bulloch 2020), as reflected by the cartoon depiction of these proteins in Figure 3.

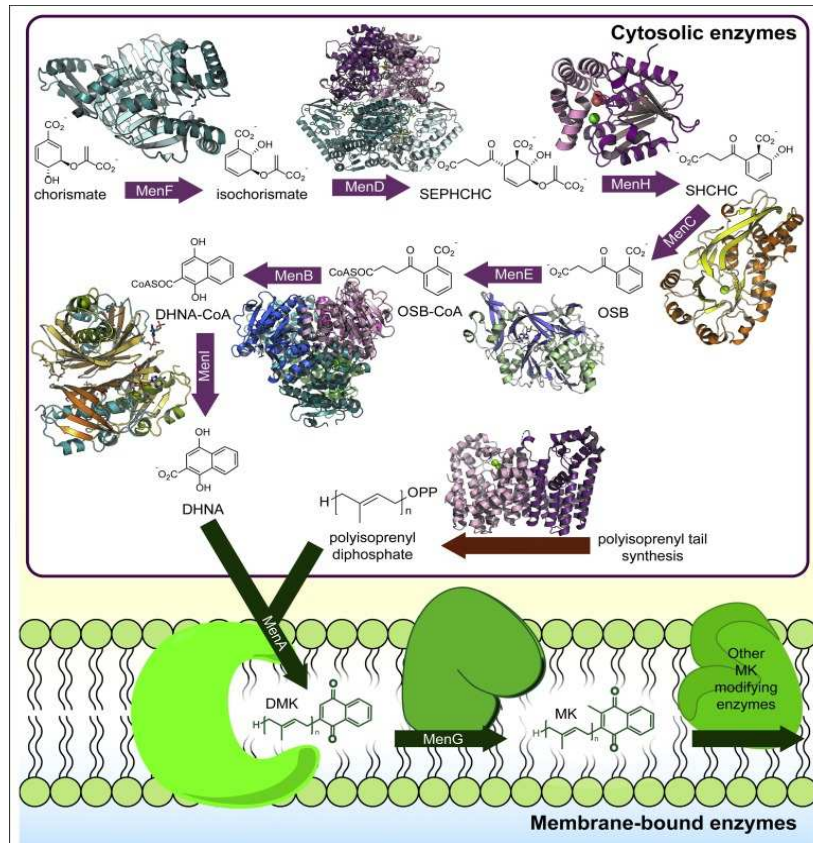


Figure 3: Depiction of the classical pathway of MK biosynthesis in bacteria. Figure adapted with permission from Johnston & Bulloch, 2020.

While depletion of MK may result in electron transport disruption, the presence of excess MK may also be deleterious to the ETS due to oxidative stress induction (Fritsch et al., 2019; Johnston & Bulloch 2020). MK biosynthesis is therefore an intricately regulated process involving signaling mechanisms that have not been fully characterized. DMK is the de-methylated product generated by MenA. Disruption of homeostatic ratios of DMK to the final MK product has been correlated to impaired microbial metabolism (Johnston et al., 2020; Puffal et al., 2018). In addition, a feedback inhibition mechanism has been proposed which involves binding of the metabolite DHNA to MenD, one of the first MK biosynthetic enzymes involved in generating the naphthoquinone precursor (Bashiri et al., 2020). Identification of signaling mechanisms

involving MK intermediates has implications for designing inhibitors of MK biosynthetic enzymes and disrupting microbial respiration.

1.1.3 Menaquinone-Associating Proteins as Antimicrobial Targets: Although the features of the microbial respiratory chain vary across species, Type II NADH : menaquinone oxidoreductase (NDH-2) has been identified as a conserved structure among pathogens such as *M. tuberculosis*, *S. aureus* and *L. monocytogenes* that has no ortholog in the mammalian ETC (Nakatani et al., 2020; Schurig-Briccio et al., 2014; Yano et al., 2014). NDH-2 couples oxidation of NADH with reduction of MK to MKH₂, resulting in the maintenance of an intermediate quinone “pool” containing both oxidized and reduced populations of MK (Schurig-Briccio et al., 2014; Sellamuthu et al., 2017; Yano et al., 2014). This process enables MKH₂-mediated electron transfer to subsequent protein complexes in the respiratory chain (Thompson et al., 2019).

Although NDH-2 does not directly regulate the generation of the proton motive force, studies indicate that its function is critical for microbial growth (Blaza et al., 2021; Schurig-Briccio et al., 2014). Subsequently, NDH-2 is a potential virulence factor and promising target for novel ETC inhibitors (Blaza et al., 2021; Shurig-Briccio et al., 2014; Nakatani et al., 2020). However, the molecular mechanisms of candidate NDH-2-inhibiting compounds are not well understood and lack NDH-2 specificity (Blaza et al., 2021). The development of antibiotic therapies targeting NDH-2 is dependent on a detailed understanding of its binding interactions and redox kinetics, which can be informed by structural and dynamic studies of its native substrates including MK.

1.1.4 Menaquinone Catalytic Mechanism: The mode of electron transfer between MK and oxidoreductases is debated due to the challenges of studying the catalytic activity

of membrane proteins in their native hydrophobic environment. In the context of NDH-2, an ETC enzyme with relevance to pathogenicity as discussed in the previous section, MK reduction is widely proposed to occur via a “ping-pong” charge transfer mechanism (Blaza et al., 2021). The ping-pong mechanism involves the binding of NADH/NAD⁺ and MK/MKH₂ to the oxidoreductase. Whether both substrates bind synchronously (two-site model) or in succession (one-site model) *in vivo* is debated (Blaza et al., 2021; Yano et al., 2014).

Although the intermolecular redox mechanism is incompletely understood, the formation of a semi-menaquinone intermediate is believed to be a key feature of MK-mediated catalysis, as determined collectively by EPR and electrochemical kinetics experiments (Grimaldi et al., 2012; Eddine et al., 2017) and supported by X-ray crystallographic structural studies which characterize MK/MKH₂ binding sites (Guan et al., 2018; Xu et al., 2020). The semi-menaquinone intermediate is defined by the formation of a radical anion once a single electron is transferred between MK and the environment, followed by transfer of the second electron (Figure 4). Formation of a semiquinone radical occurs in electrochemical assays conducted in aprotic solvent, while a synchronous 2-electron transfer mechanism is observed in aqueous solvent (Guin et al., 2011). Semiquinone radical formation has also been detected using pulsed EPR studies *in vitro*, where the semi-menaquinone was bound to a purified oxidoreductase complex (Yi et al., 2010). In the hydrophobic environment of the plasma membrane, semi-menaquinone formation is therefore an implicit characteristic of MK redox activity.

1.1.5 Role of the Isoprene Chain in Menaquinone Function: X-ray crystallographic studies of oxidoreductases bound to MK or MKH₂ have provided information regarding

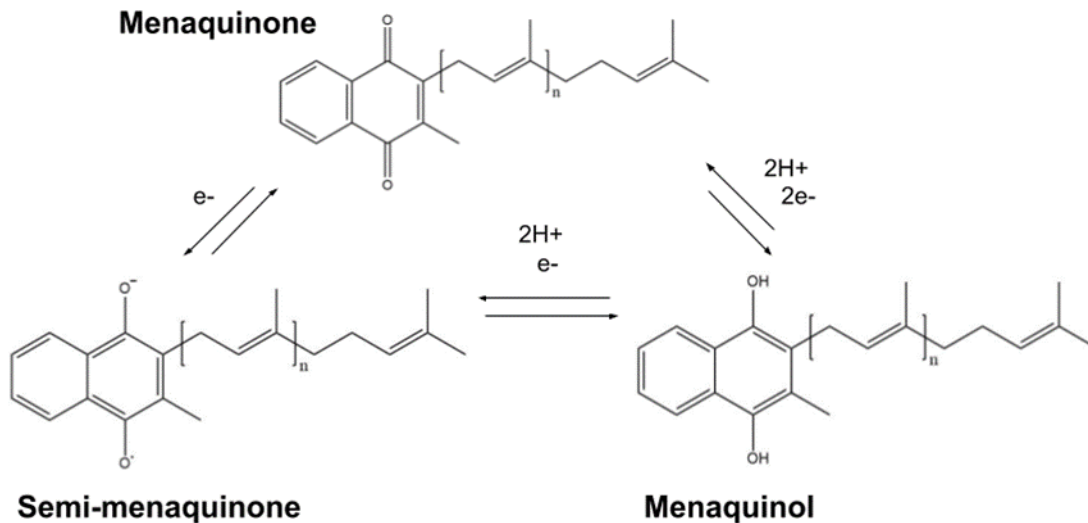


Figure 4: Depiction of semiquinone radical formation as the proposed mechanism of electron transfer between MK and its associating ETC enzymes within the phospholipid membrane. Figure created using ChemDraw Professional 16.0.

the conformation of MK during its interactions with ETC oxidoreductases (Xu et al., 2020; Guan et al., 2018). These studies have informed an understanding of MK-enzyme catalysis by characterizing naphthoquinone head group interactions with active site residues in different MK-utilizing organisms, including *D. gigas* (Guan et al., 2018) and *B. subtilis* (Xu et al., 2020). Literature searches for crystal structures of MK bound to complexes in pathogens such as *M. tuberculosis* and *S. aureus* for inclusion in this manuscript were unsuccessful. The hydrophobic nature of the isoprene chain provides challenges for its identification in crystallographic studies, and the chain is incompletely resolved in structural biology publications. In the cited manuscripts where membrane proteins were successfully co-crystallized with MK-7, only 2-3 of the 6-7 of the native isoprene units were identified using electron density mapping (Guan et al., 2018; Xu et al., 2020).

It has been inferred that the main function of the isoprene chain is to anchor MK in the hydrophobic membrane (Zhang et al., 2021). It is also possible that the isoprene chain

facilitates arrangement of MK into its redox-active conformation upon interaction with ETC enzymes. Structural studies in *B. subtilis* revealed an abundance of hydrophobic residues in the putative isoprenyl docking site and depicted the bound MK/MKH₂ molecule in an extended conformation (Xu et al., 2020). However, the isoprene side chain may also dictate MK catalytic activity by other avenues in addition to its anchoring function. Electrochemistry data produced by our laboratory indicates a statistically significant relationship between isoprene chain length, regiospecific saturation, and MK redox potential. In addition, the number of isoprene units and regiospecific reduction state have been suggested to be important for signaling, and possibly pathogen virulence (Uphadyay et al., 2015). A subsequent paper concluded that the saturation state of the β -isoprene unit of MK-9 was important for *M. tuberculosis* survival in macrophages (Uphadyay et al., 2015). However, this assertion was repealed once knockout of the enzyme MenJ, which carries out saturation of the MK-9 β -isoprene unit, was identified as the virulence factor (Kumar et al., 2020). Information regarding the relationship between MK isoprene chain length, saturation, and MK-mediated electron transport is fundamental for building a comprehensive understanding of pathogen respiratory function. Obtaining basic information regarding the properties of MK may inform studies of microbial respiration across multiple species, where enzyme catalytic residues and more general ETC pathway features may not be conserved.

1.1.6 Conformation of Quinone Derivatives in Cell Membranes: The general consensus held by the scientific community has been that isoprenoid quinones adopt a fully extended conformation within a phospholipid bilayer. However, there are multiple studies that have proposed a folded conformation as being most energetically stable

within the hydrophobic lipid environment. Computationally derived models have predicted that a folded conformation is most stable for MK variants with side chains with greater than or equal to 4 isoprene units *in vivo* (Ishihara & Sakagami 2007). MK derivatives with 3 or fewer isoprene units are indicated to assume an “extended” conformation (Ishihara & Sakagami 2007), which appears to be semi-extended when compared to the fully open conformations illustrated in most of the literature.

Ubiquinone (UBQ), the isoprenoid quinone variant found in mammalian respiratory chains and some prokaryotes, has been investigated more extensively than MK regarding its conformation and location within a membrane. Subsequently, UBQ research may inform the study of MK membrane dynamics. Molecular dynamics simulations and spectroscopic studies have suggested that UBQ adopts a bent conformation and resides within the mid-plane region of the bilayer, i.e. at the interface between inner and outer leaflets of the membrane (Lenaz et al., 2007; Samorì et al., 1992). The UBQ head group is suggested to undulate between the hydrophilic head group and hydrophobic tail of the phospholipids (Lenaz et al., 2007; Samorì et al., 1992). This conformational flexibility is believed to facilitate the binding interactions of ubiquinone with multiple mitochondrial protein complexes, since the relative location of active sites of ETC complexes is variable with respect to the hydrophilic head and hydrophobic tail regions (Lenaz et al., 2007).

1.2 Studies of Menaquinone Properties in Model Membranes: Elucidation of the fundamental interactions between MK derivatives, transmembrane proteins, and the plasma membrane is dependent on MK conformation in complex biological systems. Subsequently, model membranes are simplified systems that can be used to obtain

basic information regarding the relationship between MK structure, conformation, and its function as an electron transport molecule. The location and conformation of MK-2, a truncated MK derivative, has been previously characterized within lipid monolayers (Koehn et al., 2018). In these studies, 1D ^1H and 2D ^1H - ^1H NMR spectroscopy were used to characterize the interactions of MK-2 within reverse micelles and Langmuir phospholipids. The results of this study indicated that MK-2 assumes a folded conformation within an amphipathic monolayer. While MK-2 is not found in biological organisms, this derivative possessing 2 isoprene units was utilized based on several factors. MK-2 has slightly more rotational variability than MK-1, but less conformational flexibility than native MK derivatives with longer isoprene chains. It was therefore maintained that MK-2 would more closely resemble biologically active MK molecules, while minimizing the spectral overlap of multiple isoprene proton signals, which is an inherent challenge of ^1H NMR interpretation. Thus, a compromise was made between biological analogy and technical considerations. It was reasoned that collecting reference data regarding MK-2 properties would facilitate interpretation of subsequent experiments using more complex MK derivatives.

In the work presented herein, 1D ^1H and 2D ^1H - ^1H NMR spectroscopic methods are used to characterize the location and 3D conformation of MK-2 within a phospholipid bilayer, with the objective of expanding the biological relevance of the model membrane system. We predict that the conformation of MK-2 in a phospholipid bilayer will be similarly folded as observed in a monolayer system.

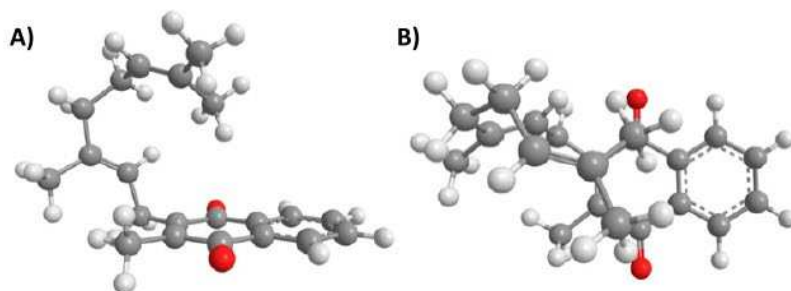


Figure 5: Conformation of MK-2 in reverse micelles from A) a side view and B) an overhead view. Relative intramolecular distances were estimated using ChemBio 3D 12.0 to conduct energy minimization and MMFF94 calculations (Koehn et al., 2018). Figure adapted from Koehn et al., 2018.

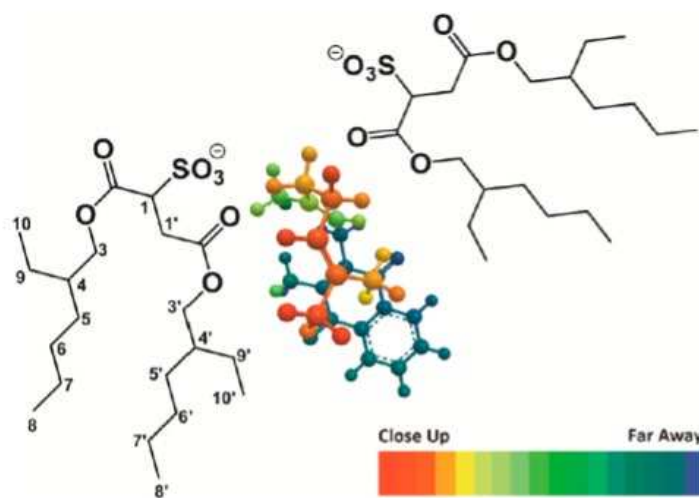


Figure 6: Proposed conformation and orientation of MK-2 in an AOT/isooctane reverse micelle. Interactions between MK-2 and the reverse micelle monolayer were determined by ^1H - ^1H NMR spectroscopic analysis of NOE interactions, and modeled using energy minimization and MMFF94 calculations (Koehn et al., 2018). Figure adapted from Koehn et al., 2018.

Chapter 2 - Utilization of Model Membranes and NMR Spectroscopy for Biologically Relevant Research

2.1 Membrane Mimetics Used to Model Biological Membranes: The study of interactions between lipids, membrane proteins, and small molecules is essential for obtaining comprehensive information regarding cell function. However, structural and functional characterization of membrane proteins and other hydrophobic biomolecules is hampered by the complexity of cell membranes (Liang et al., 2016). A hydrophobic environment is necessary for preservation of the native structure and subsequent function of membrane proteins. Further, the dynamicity of these molecules complicates the attainment of crystal structures (Mineev et al., 2016). NMR is an alternative analytical tool for structural analysis of membrane proteins and substrates. The use of NMR to study these systems requires the development of models that mimic the basic properties of cell membranes. In this chapter, examples of commonly implemented model membranes will be described, followed by a discussion of their applications toward NMR spectroscopic studies of biological systems.

2.1.1 Solvents and Self-Assembled Structures Used as Model Membranes: An array of membrane mimetics may be applied to NMR studies of biological systems, which vary in architecture and complexity. The simplest mimetics are homogenous or heterogenous mixtures of organic solvents. However, their use is limited to studying protein secondary structure or simpler molecules such as peptides, since formation of membrane protein tertiary structure is dependent on complex interactions with both the amphiphilic cell membrane and the aqueous interface (Mineev et al., 2016).

Detergents, which form monolayer or bilayer structures, are model membranes with higher analogy to the physiological environment. Reverse micelles are detergents composed of amphipathic lipids which encapsulate water molecules and are suspended in organic solvent (Fuglestad et al., 2019; Kalra & Bally, 2013). Reverse micelles have been historically implemented in NMR spectroscopic studies to encapsulate proteins of interest, resulting in faster correlation times and improved spectral resolution (Fuglestad et al., 2019; Wand et al., 1998). The applicability of reverse micelles as membrane mimetics has also been recognized (Arsene et al., 2021). Multiple studies by our laboratory have utilized reverse micelles to study the incorporation of biologically relevant compounds into a model membrane via NMR spectroscopy (Koehn et al., 2018; Peters et al., 2016, 2018).

Since cell membranes are composed of phospholipid bilayers (Warshawski et al., 2011), one disadvantage of using reverse micelles to model the cell environment is their monolayer structure. Subsequently, liposomes are used as basic model membranes with an additional degree of biological analogy. Due to their curvature and bilayer structure, liposomes are commonly used as cell membrane mimetics to study complex biological processes that are challenging to observe *in vivo* (Yeh et al., 2020). Many lipids found in the cell membranes of biological organisms spontaneously assemble into liposomes when suspended in aqueous solution. The resulting vesicle is composed of one or multiple phospholipid bilayers, which share dynamic and compositional properties with biomembranes and can be used to study biological activities. Variants of liposomal systems are used to investigate biological processes and interactions (Sebaaly et al., 2019). Since the work herein utilizes a liposome model membrane for

NMR spectroscopic studies of MK-2 conformation and location, the following sections in this chapter will discuss the preparation and formulation of liposomes.

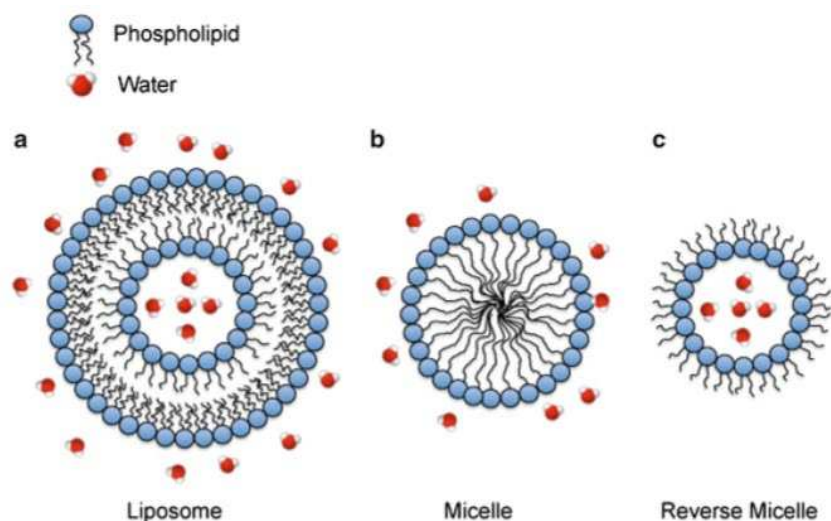


Figure 7: Comparison of liposome vs. micelle structure. Both self-assembling structures are utilized as model membrane mimetics for biological studies. Image adapted with permission from Kalra & Bally, 2013.

2.1.2 Liposome Preparation Techniques: Liposomes are classified based on diameter and are either unilamellar or multilamellar depending on the number of bilayers that constitute the vesicle. Unilamellar liposomes are appropriate for mimicking a variety of cell membranes due to their bilayer structure (Sebaaly et al., 2019), and may be prepared using relatively simple techniques. Small unilamellar vesicles (SUVs) typically range from 20-100 nm, large unilamellar vesicles (LUVs) span from 100 nm-1000 nm, and giant unilamellar vesicles (GUVs) are identified as vesicles larger than 1000 nm in diameter (Ramos, 2017, Zhang, 2017).

Selection of an appropriate method of liposome formation is dependent on the desired size of the vesicle. In this work, a thin-film hydration technique followed by extrusion was used to produce LUVs. The thin-film hydration process involves the production of a lipid cake which is produced by adding organic solvent to lyophilized lipids and then

evaporating the solvent (Zhang, 2017). For studies involving the incorporation of hydrophobic molecules into the liposomal bilayer, the protein or other molecule of interest is generally co-dissolved with the phospholipids upon addition of organic solvent during the thin-film hydration process (Rosales-Mendoza et al., 2019). The lipids are then resuspended in aqueous solvent and agitated above the phase transition temperature of the lipid (Avanti, 2021). This process results in the formation of multilamellar vesicles, which may then be extruded to produce a monodispersed solution containing unilamellar vesicles of a predetermined size (Avanti, 2021).

2.1.3 Biological Considerations for Liposome Preparation & Formulation:

Prokaryotic cells range from 0.1 to 5 μm in diameter while eukaryotic cells range from 10 to 100 μm (Fowler et al., 2013). Subsequently, the appropriate selection of a filter pore size for the extrusion process is in part dependent on the organism which the membrane mimetic is designed to simulate, since parameters such as membrane curvature may be important for study design (Baker et al., 2017). Another consideration when determining the optimal liposome size includes the analytical tool being used to study the model membrane system. NMR studies, as were implemented in this work, necessitate the use of small vesicles to achieve adequate spectral resolution and minimize line broadening (Mineev et al., 2016). These factors will be discussed in detail in later sections.

When formulating liposomes, the selection of lipid components is dependent on the biological organism being modeled and the chemical properties of the lipids.

Components of biological membranes can be generally categorized as glycerolipids, phospholipids, and sphingolipids (Casares et al., 2019). For example, phospholipids

such as phosphatidylcholine, a major component of mammalian membranes (Van der Veen et al., 2017), readily form liposomes in aqueous solution (Kalra & Bally, 2013). Conversely, phosphatidylethanolamine is a major constituent of both prokaryotic and eukaryotic membranes (Cho et al., 2021) that does not independently form a bilayer structure (Van der Brink et al., 2004). Lipid head group area/charge and environmental factors determine whether lipids will spontaneously assemble into a liposomal configuration (Van der Brink et al., 2004). A combination of lipids in a fixed ratio can be used to address this issue, and may lend additional biological relevance to a membrane model due to the heterogeneous composition of native cell membranes (Casares et al., 2019).

2.1.4 Applications of NMR Spectroscopy to Studies of Liposomal Systems:

Nuclear Magnetic Resonance (NMR) spectroscopy is an analytical technique that can be used for the structural characterization of biological systems (Marion, 2013). In NMR spectroscopy, nuclei are aligned in an applied magnetic field and excited by radiofrequency pulses. This technique is dependent on the property of nuclear spin, in which the targeted nuclei must have a non-zero spin to undergo a change in net magnetic moment when excited by radiofrequency and produce a measurable signal (Yeh et al., 2020). The rate of return of the excited nuclei to equilibrium is uniquely influenced by the molecular environment of the nuclei, regarding both atomic connectivity and proximity. Subsequently, by investigating changes in chemical shift and relaxation time, information can be inferred regarding structure and intra/intermolecular interactions. Since the nuclide of interest must have a non-zero magnetic spin, the selection of atomic nuclei for NMR analysis is limited to specific isotopes (Yeh et al.,

2020). In addition, under equilibrium conditions the populations of excited and ground state nuclei are similar. As a result, the selection of a relatively abundant isotope with a net nuclear spin is a critical consideration. For biological studies ^1H NMR is therefore commonly used, as protons are copious in biological molecules and have a net spin of $\frac{1}{2}$ (Yeh et al., 2020).

Both solution state and solid-state NMR are commonly utilized for the study of structure, dynamics, and interactions within biologically relevant systems; both have advantages and disadvantages depending on the biological property of interest. Solid state NMR yields high spectral resolution and has useful applications for structural studies of membrane proteins (Yeh et al., 2020). However, solid-state samples lack many of the dynamic properties of a physiological membrane and its membrane-bound constituents, and isotopic labeling is often necessary to mitigate spectral complexity (Liang et al., 2016). Conversely, solution state NMR is unsuitable for the study of large macromolecules due to their slow tumbling rate, which exacerbates transverse relaxation and line broadening, and reduces spectral resolution (Mineev et al., 2016). Solution state NMR is typically limited to the characterization of molecules below 50-70 kDa (Mineev et al., 2016). When designing model membranes for solution-state studies, a compromise must be made between using membrane mimetics that are physiologically relevant and ensuring that the model system is sufficiently small to be interpretable using solution state NMR. These factors were considered when selecting solution-state NMR and a relatively small vesicle size (100 nm) for the experiments presented herein. As mentioned in the previous section, a mixture of lipids is often used in membrane mimetics to be analyzed by NMR spectroscopy. However, the utility of this

approach is dependent on additional factors. For ^1H NMR, implementation of a heterogeneous liposome system may result in uninterpretable spectra due to the generation of many overlapping signals, termed “spectral crowding” (Liang et al., 2016). Since chemical shift is intrinsically related to the molecular environment, lipids possessing similar but non-identical structures will produce FIDs with minute differences in chemical shift.

Spectral crowding introduces significant, and sometimes infeasible, challenges to data interpretation. One solution is the utilization of deuterated lipids, which may significantly reduce the number of signals produced (Yeh et al., 2020). However, the expense of these deuterated formulations is a limiting factor. An alternative approach is to use non-deuterated model membranes with relatively simple lipid compositions, which imposes certain limitations to the study of cellular processes since native membranes are complex and heterogeneous structures. The variety of lipids localized to different regions of the membrane create microenvironments with variable properties that influence protein interactions and cell signaling (Casares et al., 2019). In addition, lipid composition is highly organism-dependent, as demonstrated by the diversity of membrane constituents across bacterial species (Sohlenkamp et al., 2016). Therefore, when selecting only a few lipids to model a biological membrane, the lipid composition of the organism studied and the membrane region of interest must be considered.

^1H - ^1H NOESY is a popular 2D NMR spectroscopic method that provides information regarding molecular orientation and conformation and is applied in biological studies to determine protein-ligand interactions (Liang et al., 2016) and molecular structures (Marion, 2013). Since our laboratory has used this technique extensively to study the

interactions of compounds with model membranes, NOESY was the primary 2D technique utilized in this work to assess the 3D conformation of MK-2.

Chapter 3 - Materials & Methods

3.1 Method Development

3.1.1 Optimization of Liposome Preparation and Incorporation of MK-2: Most literary sources recommend co-dissolving hydrophobic small molecules with lipids in organic solvent, purging under vacuum, and rehydrating in the desired solvent (Burgess, 1998; Rosales-Mendoza et al., 2019). However, alternative methods of sample preparation were investigated for this study. MK-2 synthesis is an extensive process involving appreciable time and resources, therefore optimizing incorporation of MK-2 into the bilayer and minimizing sample loss were of high priority. To assess the spontaneous partitioning of MK-2 into the liposomal bilayer, alternative methods of MK-2 incorporation into liposome vesicles were pursued. One method involved the preparation of liposomes by thin-film hydration, followed by dry-weight addition of MK-2 to the dried lipid cake. D₂O was then added to the sample, followed by sample heating to 45°C, mild agitation, and extrusion. The acquired spectrum showed that MK-2 protons had chemical shifts equivalent to those observed in aqueous solution, indicating unsuccessful incorporation of MK-2 into the bilayer (Figure 8). In agreement with the literature (Burgess, 1998; Rosales-Mendoza et al., 2019), it was determined that co-dissolution of lipids and MK-2 in CHCl₃, removal of the solvent, and rehydration in the desired medium before extrusion was the most effective method for incorporation of MK-2 into liposomes. This was evidenced by the relative downfield shift of the MK-2 peaks using the co-dissolution method of liposome preparation (Figure 8).

Subsequently, the co-dissolution method was utilized for the proceeding 1D and 2D NMR experiments, in which both EPC and MK-2 were dissolved in CHCl₃ before the

solvent was purged under vacuum and the MK-2/EPC mixture was resuspended in aqueous solution.

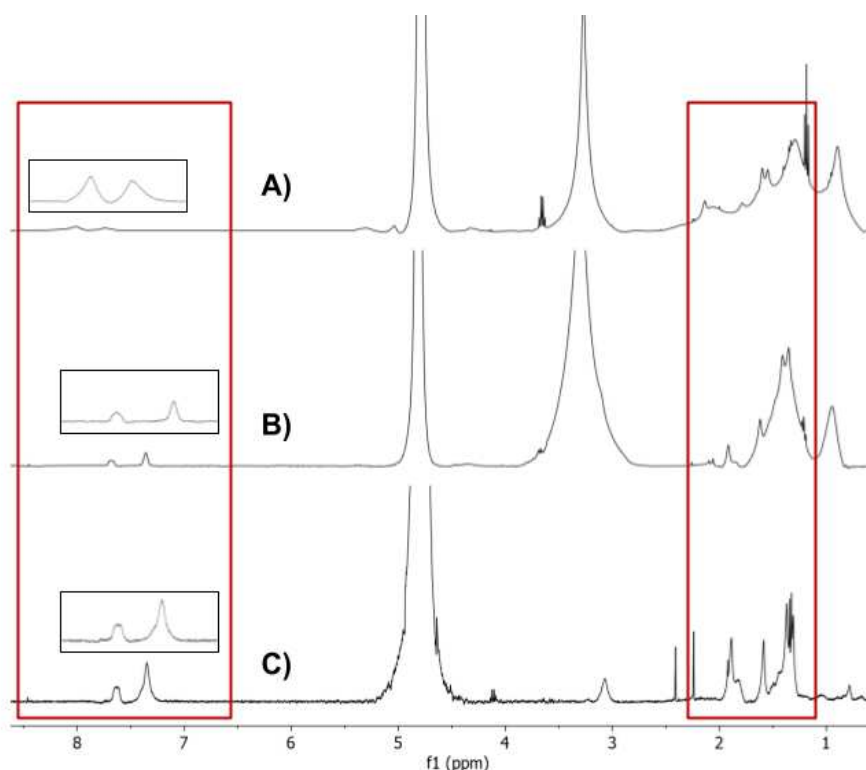


Figure 8: Comparison of methods for preparing liposome vesicles to incorporate MK-2. A) 19 mM MK-2 co-dissolved with 130 mM EPC in CHCl_3 , purged under vacuum, and rehydrated in D_2O by the thin film hydration method. The downfield chemical shift of the MK-2 peaks indicates that method A results in incorporation of MK-2 into the bilayer. B) 16 mM MK-2 added to 130 mM EPC after lipid preparation via thin film hydration. Method B results in a spectrum where the chemical shifts of MK-2 protons are similar to those observed in aqueous solution, indicating unsuccessful bilayer incorporation. C) Spectrum of an aqueous solution of 16 mM MK-2 in D_2O .

3.1.2 Liposome Sample Stability: The stability of liposomal formulations incorporating MK-2 over time was also assessed. 1D ^1H NMR spectra were recorded within 1 hour, 22 hours and 190 hours of sample preparation (Figure 9). Samples were maintained at room temperature ($\sim 25^\circ\text{C}$) between measurements. The observed decrease in MK-2 peak intensity and S/N indicated sample degradation (Figure 9). Re-extrusion of samples resulted in negligible improvements in S/N and signal resolution (data not

shown). Further, Avanti Lipids indicates that aqueous formulations of LUVs begin to undergo hydrolysis immediately upon preparation (Avanti, 2021). 2D NOESY studies were run overnight, over the course of ~3 hours. This time window was within 12 hours of sample extrusion. The spectral quality of the 2D data and 1D traces accompanying these studies indicated that appreciable degradation did not occur during the overnight NOESY experiments. It was therefore determined that the optimal window for analysis of liposome samples containing MK-2 was within <12 hours of sample preparation.

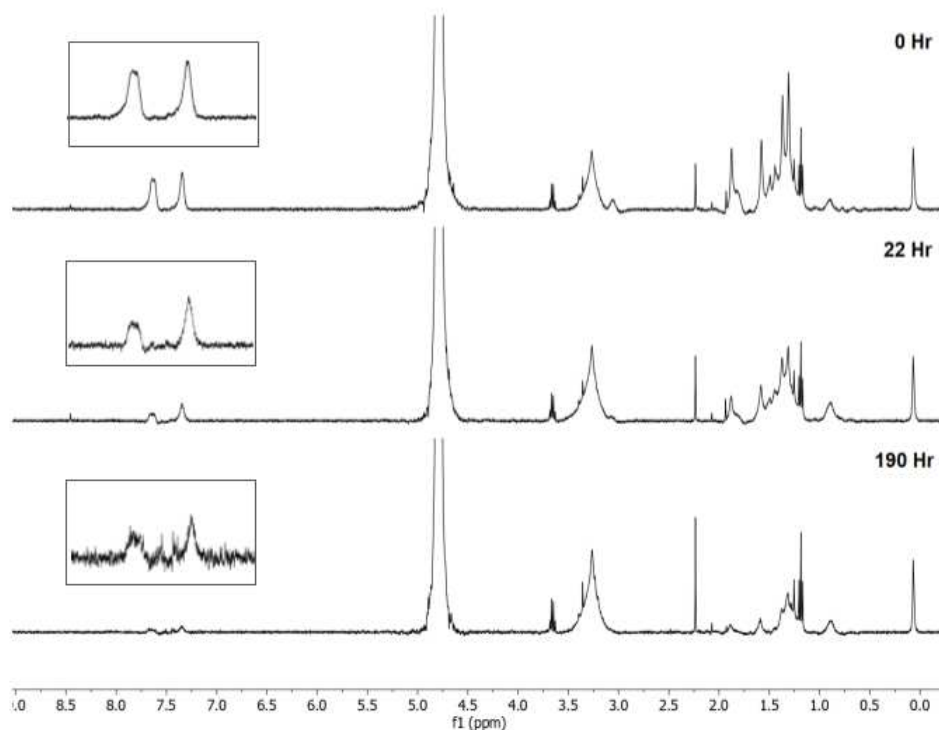


Figure 9: Assessment of liposome sample stability over time. Spectra represent the same sample and were recorded over a period of 1, 22, and 190 hours. The sample was prepared by adding 22 mM aqueous MK-2 to a dried EPC lipid film (11 mM) and extruding the mixture to obtain unilamellar vesicles, as described in the Methods section. High ratios of MK-2 : EPC were used for a separate validation test, in order to compare signal intensity ratios between MK-2 and EPC and determine the lowest lipid concentrations required for incorporation of MK-2 and sufficient signal intensity.

3.1.3 Comparison of MK-2 Derivatives for NMR Spectroscopic Studies: MK-2 was synthesized by the Crans group using a previously established procedure (Koehn et al., 2018). Our laboratory has found that two derivatives of MK-2 are produced by this method depending on the technique of the synthetic chemist. One technique generates solid yellow crystals, whereas the other technique produces a yellow-orange oil. Due to these differences in consistency and appearance, a comparison of the NMR spectral features of the two MK-2 products is discussed herein.

By comparing ^1H NMR spectra of MK-2 prepared by both synthetic techniques, it was determined that both products possess the same chemical identity (Figure 10). Additional solvent impurities and previously observed impurities with higher peak intensities are visible in the yellow-orange oil MK-2 derivative (Figure 10). This observation may be partially attributed to concentration differences, as the MK-2 spectra being compared in Figure 9 differ in concentration by a factor of 2. However, the oil form of MK-2 product appears to be less pure. NOESY spectra were also obtained using similar concentrations for both compounds (36 mM and 39 mM).

Additional NOE cross-peaks corresponding to compound impurities are observed in 36 mM NMR spectra utilizing the new method of synthesis (Figure 19). However, as evidenced by the data presented in Chapter 4 of this work, relatively consistent and repeatable 1D and 2D NMR spectroscopic data was obtained using either compound despite the presence of additional impurities. Therefore, experimental interpretation was carried out under the assumption that both derivatives of MK-2 were sufficiently similar to be comparable within the liposomal model system. One notable feature of the oil form of MK-2 is its apparent improved solubility in aqueous solution (Figure 10). Previous

publications by our laboratory have reported challenges in obtaining aqueous MK-2 spectra with high S/N due to the limited solubility of MK-2 in aqueous solution (Koehn et al., 2018). To mitigate this issue, the number of scans was increased, and the aqueous MK-2 sample was vortexed for ~1 hour. The Koehn et al. study utilized the yellow crystal form of MK-2 previously described. The aqueous MK-2 spectra obtained in the study herein utilized the oil form of MK-2 (Figure 10, Figure 20). The same strategy of increasing NMR scans (from 16 to 64) and long periods of vortexing from the Koehn et al. study was used. The aqueous MK-2 sample was heated briefly and periodically to 45°C, to facilitate MK-2 dissolution. It was found that this method produced a relatively resolved spectrum with high S/N, in comparison to spectra obtained using the solid form of MK-2 (Figure 10).

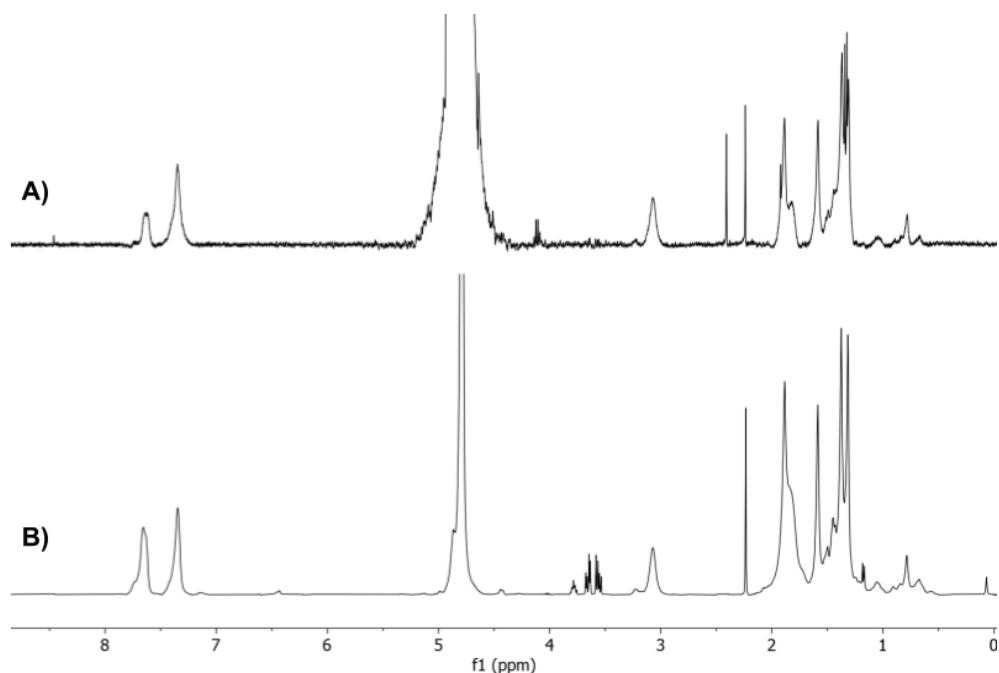


Figure 10: Comparison of the ^1H NMR spectral signature in D_2O between the solid form of MK-2 (A) and the oil form of MK-2 (B). Both compounds were synthesized by the same method described previously in literature (Koehn et al. 2018). Differences in signal intensity are attributed to differing concentrations of MK-2 in solution. Molarity values are approximate due to the limited solubility of both MK-2 derivatives in aqueous solvents.

3.2 Procedures

3.2.1 General: The following compounds and reagents were purchased and utilized at their manufactured purity: lyophilized L- α -phosphatidylcholine (Type XVI-E, $\geq 99\%$ Millipore Sigma), deuterium oxide (99.9%, Cambridge Laboratories), and 3-(Trimethylsilyl)-1-propanesulfonic acid sodium salt (97% Sigma-Aldrich). MK-2 was synthesized by the Crans Laboratory by a method previously described (Koehn et al. 2018). The pD of D₂O was adjusted using 0.1 M NaOD and DCl solutions (+0.4 pH = pD). In accordance with convention (Rubinson et al., 2017), pD will be referred to as pH for the remainder of this work (Doucette, 2021; Peters et al., 2018).

3.2.2 Preparation of Liposomes incorporated with MK-2 for NMR Spectroscopic

Studies: Large unilamellar vesicles containing MK-2 were prepared using a thin-film hydration technique followed by extrusion by hand. EPC and MK-2 were dissolved in CHCl₃ and distributed into round-bottom flasks. CHCl₃ was removed under vacuum, producing a dry film of lipids and MK-2. Purging times of 2-3 hours were implemented to maximize removal of trace solvent impurities. Liposome/MK-2 samples were rehydrated in D₂O, and heated in a 45°C water bath accompanied by rotary agitation. Unilamellar vesicles were obtained using an Avanti mini-extruder, 10 mm filter supports, and a 13 mm polycarbonate filter with a pore size of 0.1 μm . Liposome preparation methods and partial NMR spectroscopic results are included in an affiliated manuscript (Doucette, 2021).

3.2.3 Preparation of Liposomes incorporated with MK-2 for Dynamic Light

Scattering Analysis (DLS): Large unilamellar vesicles were prepared using an Avanti

mini-extruder and a polycarbonate filter as previously described for NMR analysis, with the exception that double distilled water (ddH₂O) was used as the suspension solvent *in lieu* of D₂O. Double distilled water (ddH₂O) was purified using a Barnstead E-pure system (~18 MΩ cm). Stock solutions of MK-2 (1 mg/100 μL) and EPC (1 mg/10 μL) were prepared by dissolving each compound separately in CHCl₃. Samples containing 0,4,6,8, and 12% MK-2 (w/w%) and 100, 96, 94, and 88% EPC were prepared by adding allotted volumes of each stock solution to round bottom flasks, for a total solution concentration of 20 mg/mL in each flask. DLS methods and results are included in an affiliated manuscript (Doucette, 2021).

3.2.4 NMR Spectroscopic Studies: 1D ¹H and 2D ¹H-¹H NMR were performed using a Bruker Model NEO 400 operating at 400 MHz. FIDs were recorded using similar parameters implemented in the Crans Laboratory to study related quinone-lipid model systems (Koehn et al. 2018). Chemical shift values were reported in units of ppm. Signals were referenced using the HOD internal solvent peak and the TMA peak as internal references. The consistency in chemical shift of these signals was verified by obtaining FIDs of multiple pure liposome samples and liposome samples incorporating MK-2. When the D₂O solvent peak was referenced to 4.79 ppm, the TMA signal was observed at 3.26 ppm independently of the chemical environment.

3.2.5 1D ¹H and 2D ¹H-¹H NMR Studies of MK-2 in Liposomes: 1D ¹H NMR spectra were recorded at 25°C using 16 scans, a 1.0 s relaxation delay, and a 45° pulse angle. 2D NOESY and ROESY spectra were recorded at 25°C using 256 transients, 16 scans in the f1 domain, a 200 ms mixing time, a 45° pulse angle, and a 2.0 s relaxation delay. General parameters were adapted from those utilized for previous experiments from our

research group involving the interactions of MK-2 with model membranes (Koehn et al., 2018).

3.2.6 1D ^1H T_1 Relaxation Experiments: 1D ^1H NMR spectra were recorded at 25°C using 2 scans, 2 dummy scans, and a 15.0 s relaxation delay. Multiple variable delay pulse sequences were used depending on the nuclear environment of interest. Plot points used for T_1 calculations were selected depending on the goodness of fit to an exponential curve. T_1 values were determined with the Data Analysis feature in MestreNova 14.2, using a three-parameter exponential fit.

3.2.7 DLS Studies: DLS analysis was performed at 25° using a Zetasizer Nano-ZS instrument. A 600 s equilibration time preceded each DLS measurement, followed by 10 acquisitions. 15 scans were recorded for each acquisition. PDI, zeta potential, and vesicle size values presented in this study were determined using Zetasizer software. All calculated values are averages of triplicate measurements, as referenced in an affiliated manuscript (Doucette, 2021) and a publication by our research group (Peters et al. 2016).

3.2.8 Molecular Mechanics Analysis: To visualize approximate MK-2 conformations, molecular models of MK-2 were created using ChemBio 3D Software (Koehn et al., 2018). MK-2 rotational bond angles were adjusted manually to produce a molecular conformation in consensus with the intramolecular distances determined by obtained 2D ^1H - ^1H NOESY spectra. A MM2 molecular mechanics energy minimization calculation was performed for dihedral angles.

3.2.9. Statistical Analysis: For DLS analysis, statistical analysis was performed on Graphpad Prism 84.3 using a standard t-test and one-way ANOVA. A p-value < 0.05

was used as the limit for statistical significance. The mentioned statistical methods and results are included in an affiliated manuscript (Doucette, 2021). For T_1 experiments, standard error values were calculated automatically in MestreNova 14.2 using a three-parameter exponential fit and standard deviation values were calculated using Microsoft Excel.

Chapter 4 - Results & Discussion

4.1 1D ^1H NMR Spectroscopic Analysis of MK-2 in Liposome Vesicles: MK-2 was examined within a liposomal model system using 1D ^1H NMR spectroscopy. Baseline data was obtained by recording ^1H NMR spectra of MK-2 in D_2O . For the purposes of spectral interpretation, MK-2 proton assignments were made based on the predicted chemical shift of proton signals and confirmed by referencing a previous study describing the spectral signature of MK-2 in D_2O (Koehn et al., 2018) (Figure 11). A control spectrum of empty L-alpha-phosphatidylcholine (EPC) liposome vesicles in D_2O was also recorded (Figure 12). Peak assignments were determined based on comparisons to an existing publication containing 1D ^1H NMR spectra of liposomes with a closely homologous lipid structure (Cardia et al., 2019).

To confirm the formation of liposomes and monodispersity of the samples, the hydrodynamic radius of the liposome vesicles was measured using Dynamic Light Scattering (DLS). This was performed by measuring the sizes of empty liposome vesicles and liposomes incorporating increasing concentrations of MK-2. The DLS results indicated that the samples were relatively monodispersed in solution, and that MK-2 incorporation had effects on vesicle size that were statistically non-significant (Appendices Table S1). After annotation of the relevant proton signals in the control MK-2 and EPC spectra, a titration assay was performed to investigate incorporation of MK-2 into the liposomal bilayer (Figure 13). Samples composed of fixed concentrations of EPC (130 mM) and increasing concentrations of MK-2 (13, 19, 26, 39 mM) were

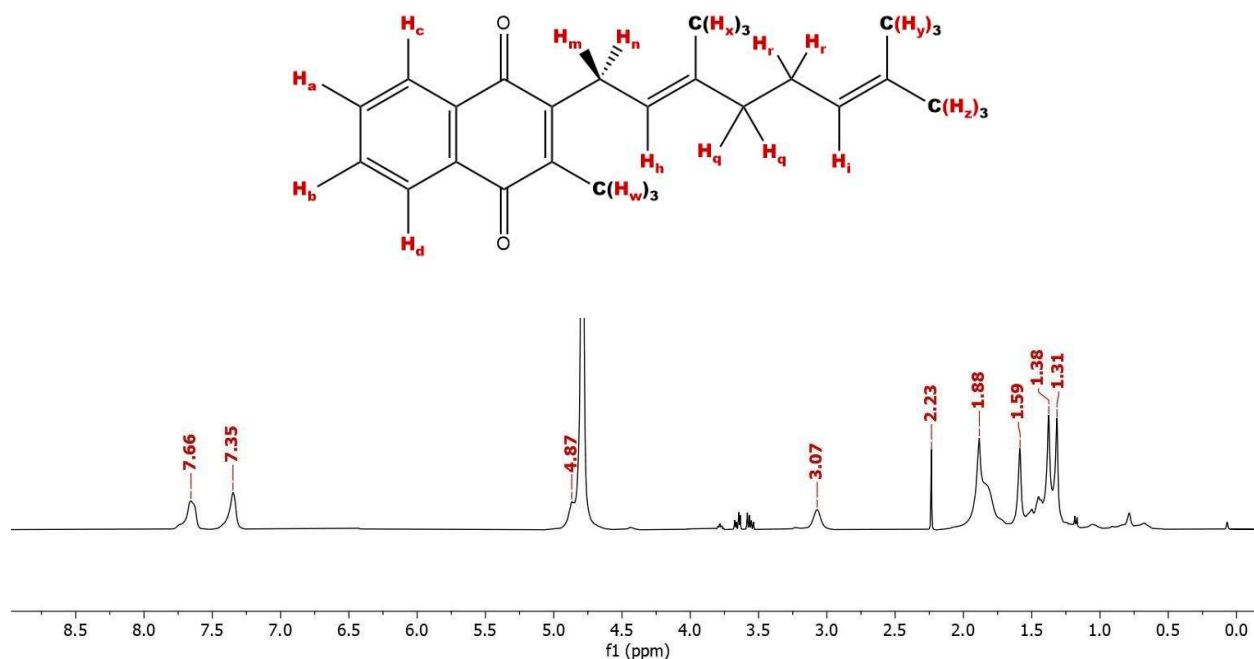


Figure 11: The structure of MK-2, a synthetic truncated menaquinone derivative, and the 1D ¹H NMR spectrum of MK-2 (39 mM) in D₂O. Protons are lettered to facilitate NMR signal annotation and spectral interpretation. Lettering scheme is adapted from both Koehn et al., 2018; and a collaborative project (Doucette, 2021).

Table 1: Chemical shift approximations corresponding to the MK-2 proton signals in Figure 11.

Chemical Shift (ppm)	Assignment
7.66	H _a /b
7.35	H _c /d
4.87	H _h /i
3.07	H _m /n
2.23	Acetone (Impurity)
1.88	H _w , H _r /q
1.59	H _x
1.38	H _z
1.31	H _y

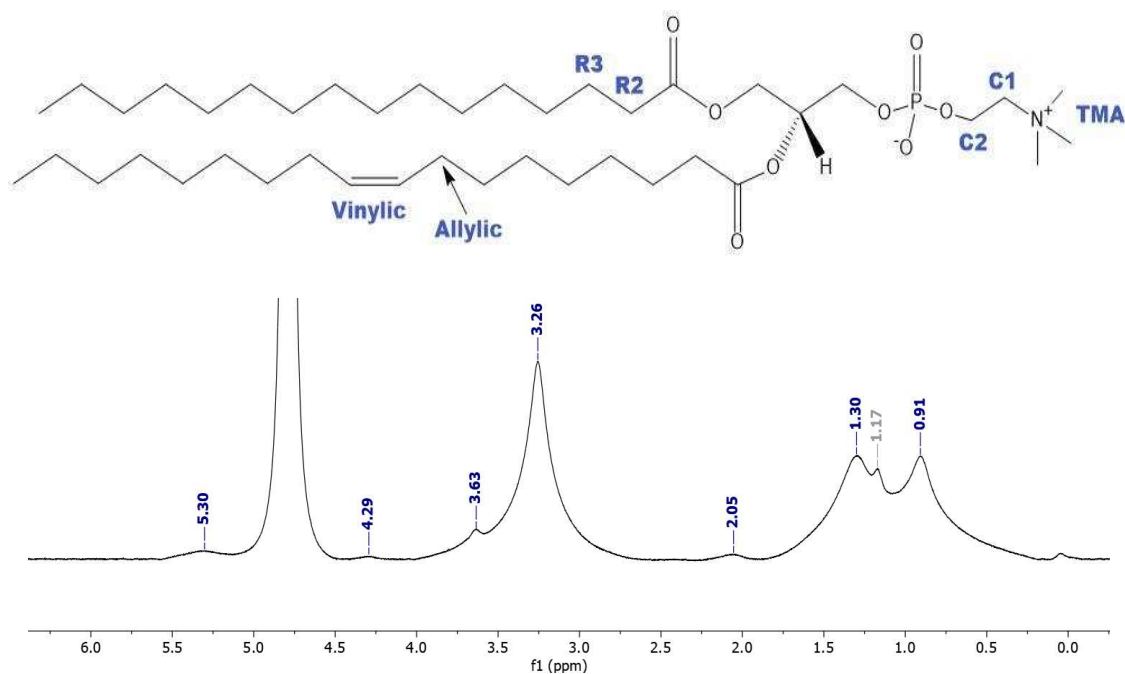


Figure 12: The structure of L- α -phosphatidylcholine isolated from egg yolk (EPC) and the 1D ^1H NMR spectrum of EPC in D₂O. Labels corresponding to structural features are included to facilitate NMR signal annotation and spectral interpretation. Lettering scheme is adapted from a collaborative project (Doucette, 2021).

Table 2: Chemical shift approximations corresponding to the EPC proton signals in Figure 12.

Chemical Shift (ppm)	Assignment
5.30	Vinylic, G2
4.29	C2
3.63	C1
3.26	TMA
2.05	Allylic
1.30	R-CH ₂
1.17	Ethanol (impurity)
0.91	R-CH ₃

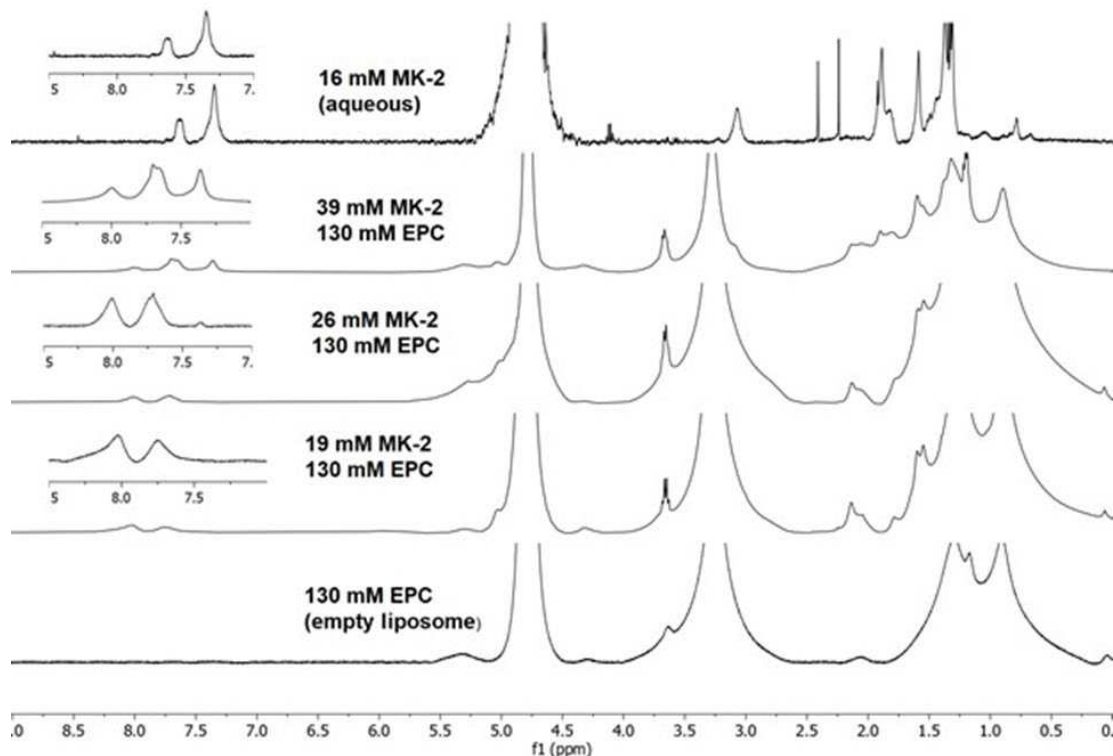


Figure 13: 1D ^1H NMR spectra of EPC liposomes titrated with increasing concentrations of MK-2. As MK-2 concentration increases, a new peak appears at ~ 7.36 ppm. The new signal is similar in chemical shift to aromatic signal H_{c/d} (7.35 ppm) of the aqueous control spectrum, suggesting emergence of a subpopulation of MK-2 at the aqueous interface.

produced using the thin-film hydration procedure as described in the Methods section of this manuscript. The chemical shifts of the proton signals in each spectrum were compared. The abundance of lipid peaks in the upfield region of the spectra complicate MK-2 signal assignment and interpretation at higher concentrations of MK-2 (26-39 mM); however, the 13-19 mM MK-2 spectra exhibit a more resolved peak pattern with high similarity to the aqueous MK-2 spectrum. As a result, the relative downfield shift of MK-2 peaks relative to the control was readily identified in the 13-19 mM spectra (Figure 13). With respect to the control aqueous MK-2 spectrum, a downfield shift of all MK-2 peaks is observed in the 13 mM MK-2 liposomal spectrum. This downfield shift of MK-2 signals is particularly pronounced in the aromatic region of the spectra (~ 6.5 - 8.0 ppm)

due to the lack of overlapping signals corresponding to lipid peaks. From this preliminary analysis, we predicted that MK-2 was incorporated into the bilayer in proximity with the charged phosphate and trimethylammonium (TMA) regions of the phospholipids, which would be expected to reduce electron shielding of the aromatic protons.

As previously discussed, the downfield shift of liposomal MK-2 samples relative to aqueous MK-2 is indicative of increased electron density in the molecular environment. This suggests that MK-2 is proximal to the zwitterionic head group region of the phospholipid bilayer. Since this downfield shift is ubiquitous among all MK-2 signals in a spectrum, it can be inferred that interactions are stronger between MK-2 and the phospholipid head groups than the bulk water pool or the hydrophobic tail region of the bilayer. Further, it may indicate that MK-2 does not associate with the phospholipid tails in this system. Considering the hydrophobicity of MK-2 and the biological function of menaquinone as a membrane-bound molecule, this result would be in divergence with expectations. However, compared to most native menaquinone analogs which are highly hydrophobic due to their 6-10 repeating isoprene units (Nowicka et al., 2010), the truncated isoprene chain of MK-2 lends this molecule increased polarity, which may contribute to a lack of thermodynamically driven burying of the isoprene chain into the bilayer. Alternatively, the de-shielding effect could indicate localization of MK-2 near the allylic region of the phospholipid tail. This possibility would be more consistent with previous studies by our laboratory and the relative hydrophobicity of MK-2, as indicated by the limited solubility of MK-2 in D₂O. Experimental factors such as the sample preparation method are also possible contributors to the potential lack of MK-2

association with the hydrophobic region of the bilayer. However, the thin-film hydration method used was consistent with both literary precedents (Rosales-Mendoza et al., 2019) and manufacturer instructions (Avanti, 2021), suggesting that the observed chemical shift change is attributed to thermodynamic effects independent of sample preparation technique.

At higher concentrations of MK-2 (26-39 mM), an additional peak emerges at ~8.0 ppm (Figure 13). This peak is first visible at 26 mM MK-2; however, the signal area and intensity are not sufficient to obtain a measurable integration value. At 39 mM MK-2, the signal manifests as a distinct peak with a calculable area. The relative integration with respect to the two downfield aromatic peaks at 8.0 and 7.65 ppm was determined to be a 1:2:1 ratio. These integration ratios are consistent with the observation of a shoulder appearing downfield on the 7.65 ppm peak at higher concentrations, suggesting spectral overlap of two distinct signals. The chemical shift of the emerging peak is consistent with the shift of the H_{c/d} peak of the aqueous MK-2 sample.

Comprehensively, these observations implicate the emergence of an aqueous MK-2 subspecies at ratios of MK-2 : EPC equal to or exceeding 1:5.

4.2 2D ¹H-¹H NMR Spectroscopic Analysis of MK-2 in Liposome Vesicles: The results of the 1D NMR titration experiment indicate that 1) the polarity of the molecular environment of MK-2 increases in the context of a liposomal system, and 2) an aqueous subspecies of MK-2 forms at higher ratios of MK-2 : lipid. 2D NOESY ¹H-¹H NMR spectroscopy was used to further investigate the conformation and location of MK-2 within the model membrane system. Samples were made using the thin-film hydration method described for the 1D NMR experiments, at ratios of 19 mM MK-2 : 130 mM EPC

and 39 mM MK-2 : 130 mM EPC. These concentrations were selected based on the results of the titration assay, in which a signal at 8.0 ppm is observed at higher MK-2 concentrations and its intensity increases as a function of molarity, while the 8.0 ppm signal is absent at ≤ 19 mM MK-2. We anticipated that both the 19 and 39 mM concentrations would be sufficiently high to produce NOE signals. We also predicted that the two spectra would have distinct NOE signatures, which could be compared to assess concentration-dependent changes in the chemical environment of MK-2.

4.3 ^1H - ^1H NOESY NMR of Liposomes Incorporating 19 mM MK-2: A signal at 8.0 ppm is absent from the NOESY spectrum of 19 mM MK-2 in 130 mM EPC (Figure 14), which is consistent with results from the preceding 1D experiments. NOE cross peaks are present between the aromatic protons $\text{H}_{a/b}$ (8.01 ppm), $\text{H}_{c/d}$ (7.75 ppm), and proximal isoprene protons $\text{H}_{q/r}$ (2.13 ppm) and H_x (1.78 ppm) (Figure 14). Although the peak at 2.13 ppm could correspond to H_w based on its chemical shift, this NOE interaction is unlikely due to the rotational immobility of the C- H_w bond. ChemBio 3D analysis indicates that H_w is within 4.9 Å of H_d , but is 7.1 Å from H_b (data not shown), which is considered to exceed the distance limits of an interproton NOE signal (Clare, 2016). NOE peaks are also shown between $\text{H}_{a/b}$, $\text{H}_{c/d}$ and the terminal methyl protons $\text{H}_{z/y}$ (Figure 14). The relative intensity of the NOE cross peaks indicates that $\text{H}_{r/q}$ are closer in through-space proximity to the aromatic protons than the more distal isoprene protons H_x , H_y , and H_z . In the 19 mM MK-2 NOESY spectrum, the $\text{H}_{r/q}$ peak at 2.13 ppm overlaps closely with the putative allylic peak of the phospholipids (2.07 ppm) (Figure 14). Background subtraction was attempted both manually and using the Arithmetic function in MestreNova, to confirm the identities of the closely overlapping

peaks. However, this analysis was inconclusive due to the inconsistent intensity ratios of individual signals between the liposomal MK-2 spectrum and the control liposome spectrum being subtracted. Subsequently, NOE cross peak patterns were used to distinguish MK-2 and lipid peaks. Since NOE cross talk is typically stronger and more frequent between protons on the same molecule (Anglister et al., 2016), analysis of cross talk between the lipid peaks supports our peak assignments. Distinct cross peaks are present between the signal at 2.07 ppm and multiple well-resolved lipid signals such

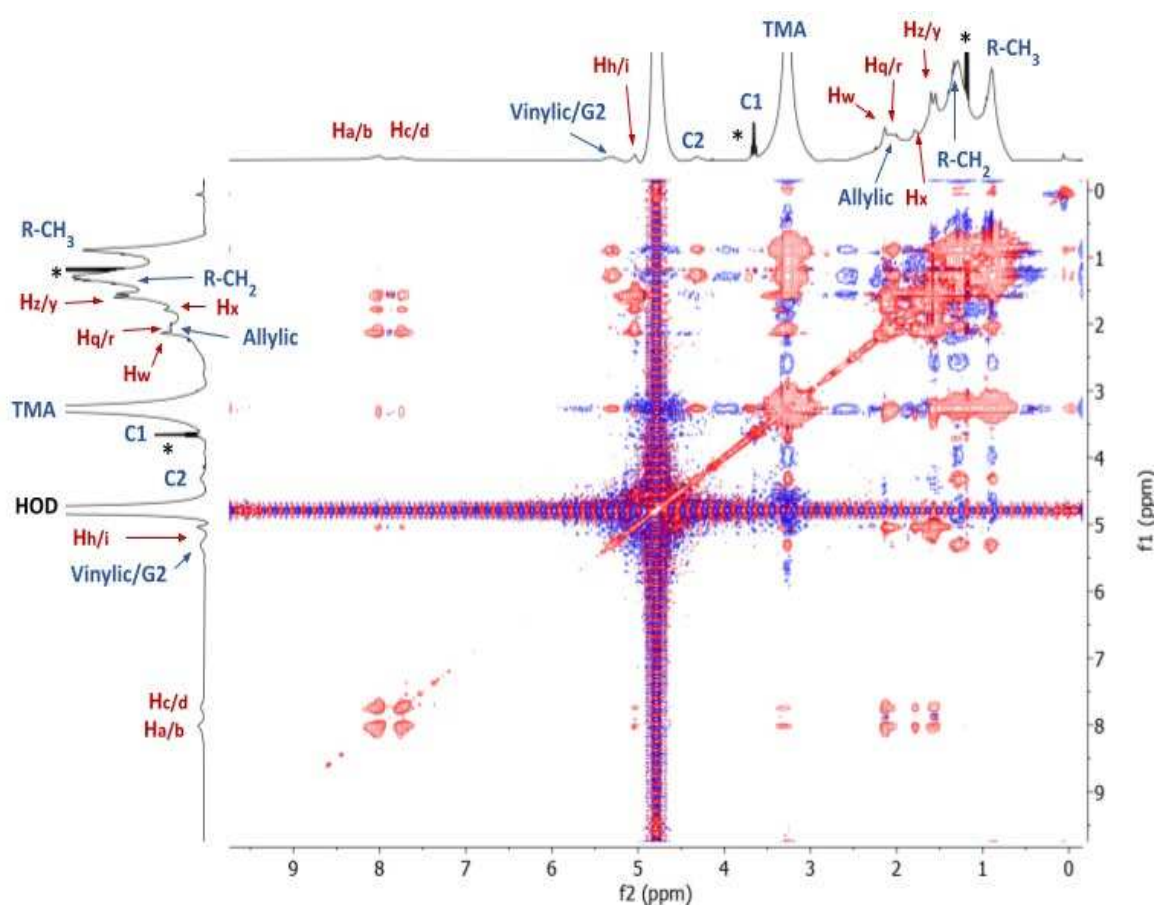


Figure 14: ^1H - ^1H 2D NOESY NMR spectrum of 19 mM MK-2 in 130 mM EPC liposomes at 25°C. Cross talk between the aromatic protons and isoprenyl protons suggests a folded conformation of MK-2 when interactions with the lipid bilayer are present. Asterisks (*) indicate impurities. Spectrum adapted with modification from a collaborative project (Doucette, 2021).

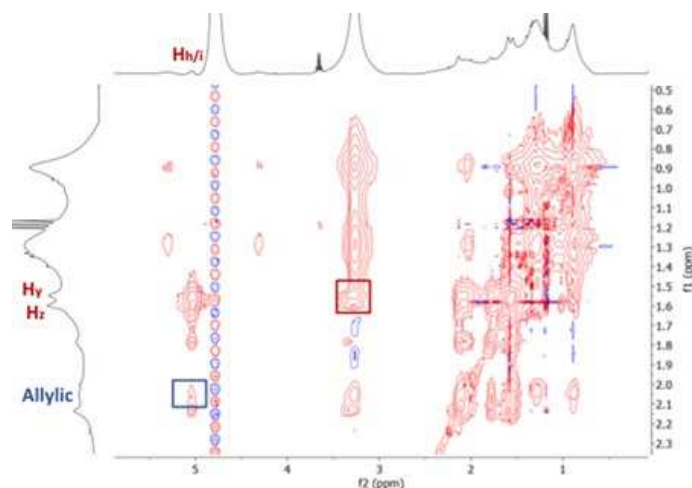


Figure 15: Partial NOESY spectrum of 19 mM MK-2 in liposomes at 25°C. The spectrum indicates intermolecular crosstalk between terminal methyl protons Hy, Hz, and the TMA peak (red), and potential interactions between Hh/i of the isoprene chain and the allylic region of the EPC liposomes (blue).

as the G2/Vinylic peak (5.30 ppm), and R-CH₃ (0.90 ppm) (Figure 14, Figure 15).

Additionally, the peak at 2.07 ppm displays cross talk with MK-2 peak Hh/i at 5.05 ppm (Figure 15). This NOE interaction suggests that this region of the MK-2 alkyl chain is localized to the allylic region of the liposome bilayer. Additional intermolecular interactions are observed between the trimethylammonium (TMA) signal and the Hy, Hz peaks at 1.54 and 1.60 ppm (Figure 15), suggesting proximity between the terminal methyl groups of MK-2 and the phospholipid head groups of the model membrane.

In all NOESY spectra recorded for this study, relatively few cross peaks are observed between MK-2 and phospholipid protons. This finding is not unusual, as intermolecular NOE interactions are typically weak due to the relationship between NOE signals and the internuclear distance (r). NOE strength is inversely proportional to the r^6 value, therefore the signal decreases with intermolecular distance (Anglister et al., 2016). As a result, intramolecular interactions compose the majority of cross peaks in a NOESY

spectrum (Anglister et al., 2016). In addition, NOE signal strength is dependent on the molecular tumbling rate, which is directly related to molecular size (Edison et al., 2010). In this study, analysis of chemical shift values and changes in relaxation time were therefore used as additional indicators of intermolecular interactions.

Together, the results from the 19 mM MK-2 spectrum indicate that MK-2 assumes a folded conformation in the liposomal bilayer. Since NOE interactions are generally considered to be observed between nuclei within 5-6 Å (Clare, 2016), NOE cross peaks between the aromatic protons and the isoprenyl protons would not be observed if the conformation of MK-2 was extended in the phospholipid environment. This conformational analysis of MK-2 is in agreement with previous research conducted in our laboratory, in which both MK-2 was concluded to assume a U-shaped conformation in a lipid monolayer (Koehn et al., 2018). This study demonstrated NOE interactions between different regions of the isoprene chain. However, in these previous experiments no interactions between the naphthoquinone ring and alkyl protons were observed. In the spectra presented herein, distinct NOEs are shown between the aromatic protons and alkyl protons. It is possible that this is attributed to environmental differences. The preceding experiments characterizing MK-2 were performed in organic solvent and/or reverse micelles. The viscosities of the D₂O solvent and EPC liposomes used in the current study differ from the chemical environments used previously, and may have affected the correlation time, resulting in the appearance of additional NOEs in the aromatic region. Alternatively, these additional cross-peaks may indicate that MK-2 assumes a more tightly folded conformation in liposomes than previously observed in reverse micelles and organic solvents.

4.4 ^1H - ^1H 2D NOESY NMR of Liposomes Incorporating 39 mM MK-2: To determine the identity and chemical environment of the additional peaks emerging at higher concentrations of MK-2 in the 1D ^1H NMR spectra, a 2D NOESY NMR spectrum was obtained using a liposome sample containing 39 mM MK-2 (Figure 16). Additional NOE interactions are observed in this spectrum that are absent from the 19 mM 2D spectrum. New cross peaks are observed at 7.35 ppm, upfield of the previously characterized $\text{H}_{a/b}$ and $\text{H}_{c/d}$ signals observed at 8.0 and 7.75 ppm in the 19 mM MK-2 1D and 2D spectra. The 7.35 ppm peak interacts with protons at 1.58, 1.88, and 3.07 ppm (Figure 16, Figure 17). These chemical shifts correspond to the chemical shifts of H_z , H_x , and $\text{H}_{m/n}$ observed in the 1D aqueous MK-2 spectrum. In addition, there are NOEs between the solvent (HOD) peak and signals with chemical shifts equivalent to the aqueous MK-2 species. Cross talk is shown between the HOD peak and the 7.35 ppm peak (aqueous $\text{H}_{c/d}$), but absent for the downfield aromatic peaks at 8.0 and 7.75 ppm (Figure 17). An additional NOE signal is present between the HOD peak and a peak at approximately 7.62 ppm (Figure 17), which is similar to the chemical shift of aqueous $\text{H}_{a/b}$ in the control MK-2 spectra. The spectral signature observed in the 39 mM spectrum is consistent with our conjecture that an aqueous subspecies of MK-2 is present at higher concentrations of MK-2 in the liposomal system.

One notable feature of the 39 mM MK-2 spectrum is the appearance of a NOE at 2.04 ppm. Despite small differences in chemical shift, consistencies in spectral pattern indicate that this signal likely corresponds to the allylic peak of EPC, which was identified in the 19 mM spectrum at 2.07 ppm. In the 39 mM spectrum, the presumed allylic peak at 2.04 ppm interacts with the $\text{H}_{h/i}$ peak at 5.03 ppm (Figure 18). This NOE

is consistent with observations from the 16 mM spectrum, and reinforces the interpretation that the mid-alkyl region of MK-2 localizes to the allylic region of the liposome bilayer. In addition, a weak NOE is observable between Ha/b and the TMA peak of the EPC lipids (Figure 18). Together, these observations support the interpretation that MK-2 is incorporated into the bilayer, and that a folded conformation is adopted, with the aromatic protons and sections of the isoprene chain in close proximity to the polar head groups of the model membrane.

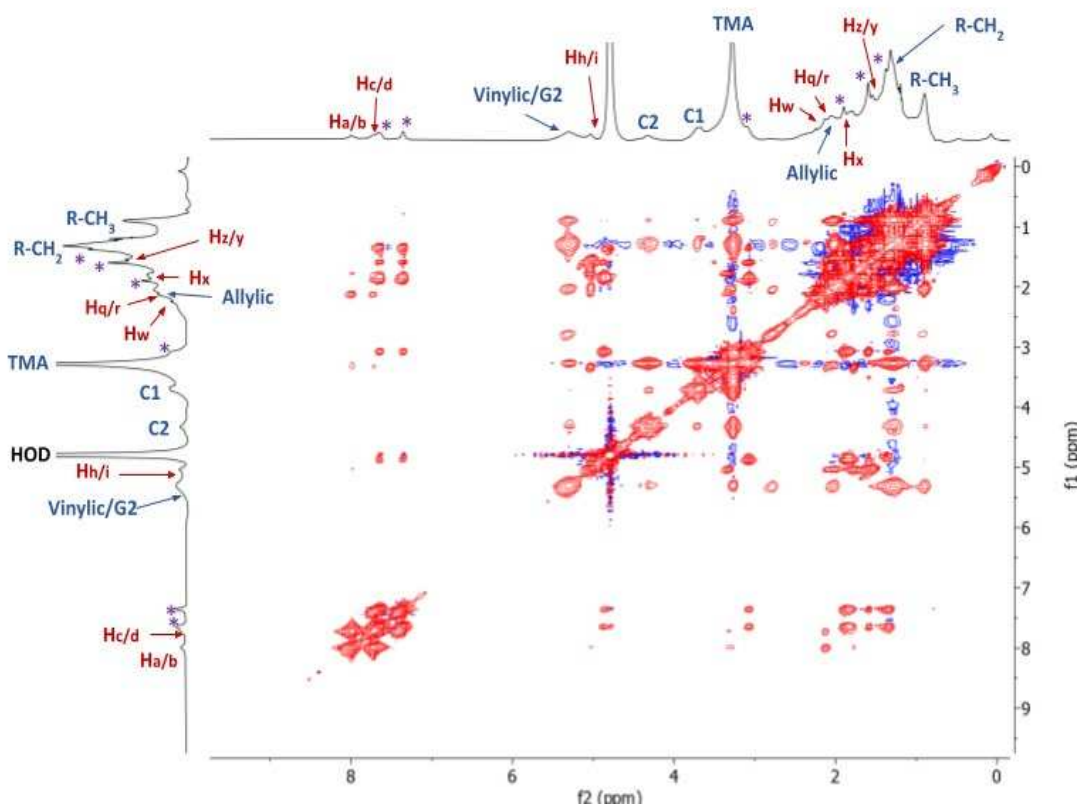


Figure 16: ^1H - ^1H 2D NOESY NMR spectrum of 39 mM MK-2 in 130 mM EPC liposomes at 25°C. New peaks in the upfield aromatic region of the spectrum are marked with asterisks (*) and are equivalent in chemical shift and spectral signature to those observed for MK-2 in an aqueous spectrum. Spectrum adapted with modification from a collaborative project (Doucette, 2021).

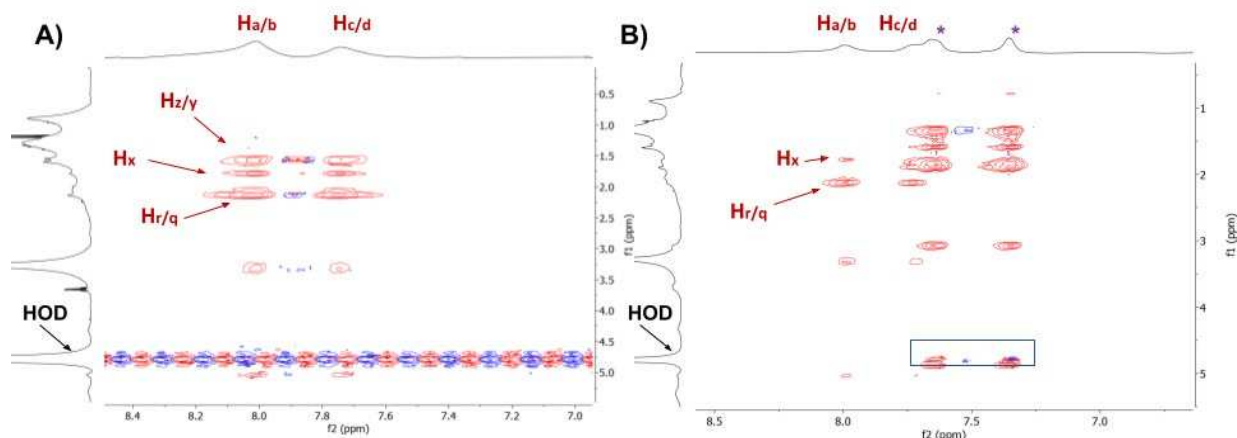


Figure 17: Comparison of intramolecular interactions between the aromatic and alkyl protons of MK-2 in liposomes incorporating 19 mM (A) and 39 mM (B) MK-2 at 25°C. Analysis reveals that the NOE peaks at approximately 7.35-4.79 ppm and 7.65-4.79 ppm partially overlap with MK-2 peaks, but are distinct signals that indicate cross-talk between these aromatic protons and the aqueous solvent. Purple asterisks (*) represent 1D traces of aromatic peaks corresponding to MK-2 molecules interacting with aqueous solvent. Spectra adapted with modification from a collaborative project (Doucette, 2021).

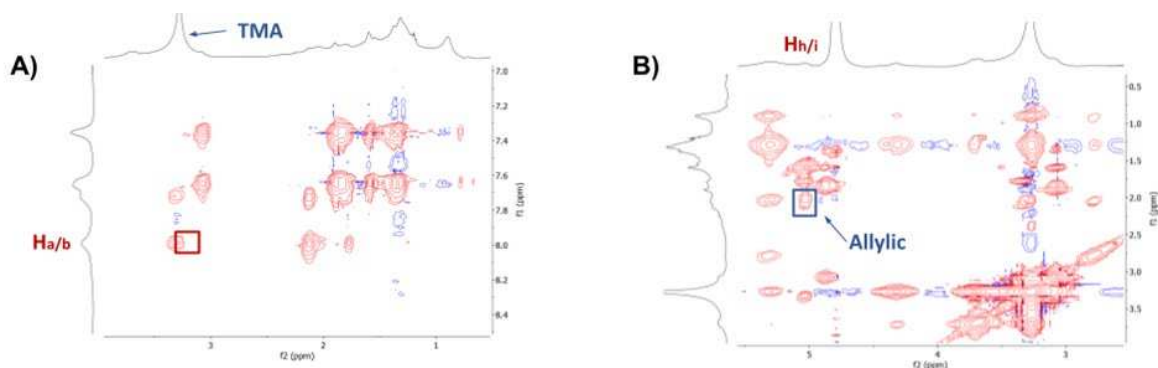


Figure 18: Partial NOESY spectra of 39 mM MK-2 in liposomes at 25°C. A) Highlighted region may indicate intermolecular cross talk between membrane-bound aromatic protons $H_{a/b}$ and the TMA peak (red). B) Highlighted region indicates cross talk between the $H_{h/i}$ protons of the MK-2 alkyl chain and the allylic peak of the EPC phospholipids (blue). Assignment of the peak at 2.04 ppm to the lipid hydrocarbon chain is supported by NOEs between the peak at 2.04 ppm and Vinylic/G2 (5.30 ppm) and TMA (3.26 ppm) lipid peaks that were identified in the EPC control spectrum. Spectra adapted with modification from a collaborative project (Doucette, 2021).

4.5 ^1H - ^1H 2D NOESY NMR of Liposomes Incorporating 36 mM MK-2: The 1D and 2D spectra depicted in preceding sections were obtained using the solid crystal form of MK-2 for sample preparation. To verify the repeatability of these results using the oil form of MK-2 generated by the alternative technique (Chapter 3.1.3), an additional NOESY spectrum was taken using a similar concentration of MK-2. The MK-2 liposome sample was prepared using 36 mM MK-2 and 130 mM EPC, and an additional NOESY spectrum was taken. Identical parameters and preparation procedures were used, with the exception that the NMR tube was degassed with argon with the intent of optimizing spectral resolution via the removal of dissolved O_2 . The subsequent 2D spectrum yielded a spectral signature similar to that observed in samples containing 39 mM of the solid MK-2 derivative (Figure 19), albeit several NOEs are not visible due to differences in concentration. In addition, this 36 mM spectrum exhibited improved resolution of several MK-2 peaks, allowing liposomal H_y and H_z , which overlap closely in chemical shift, to be differentiated (Appendices S2). Analysis of NOE intensities suggests that H_y and H_z are equidistant from the aromatic protons.

4.6 ^1H - ^1H 2D NOESY NMR of 39 mM MK-2 in Aqueous Solvent: While MK-2 is known to reside in the amphiphilic environment of a lipid bilayer, the nature of the liposomal system used in this study prompted the recording of control spectra of MK-2 in aqueous solution. This was performed for both quality control purposes, and to compare MK-2 conformation based on differences in environmental viscosity and polarity. Figure 20 depicts the 2D NOESY spectrum of approximately 39 mM MK-2 suspended in D_2O . Cross peaks are present between the aromatic protons $\text{H}_{a/b}$, $\text{H}_{c/d}$ and each of the isoprene proton groups.

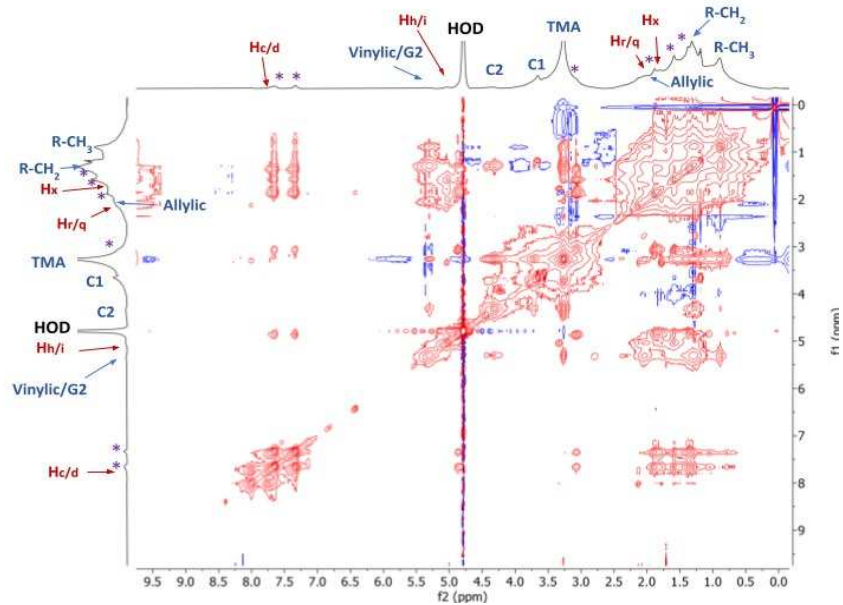


Figure 19: ^1H - ^1H 2D NOESY NMR spectrum of 36 mM MK-2 in 130 mM EPC liposomes at 25°C. Purple asterisks (*) represent peaks corresponding to MK-2 molecules interacting with aqueous solvent.

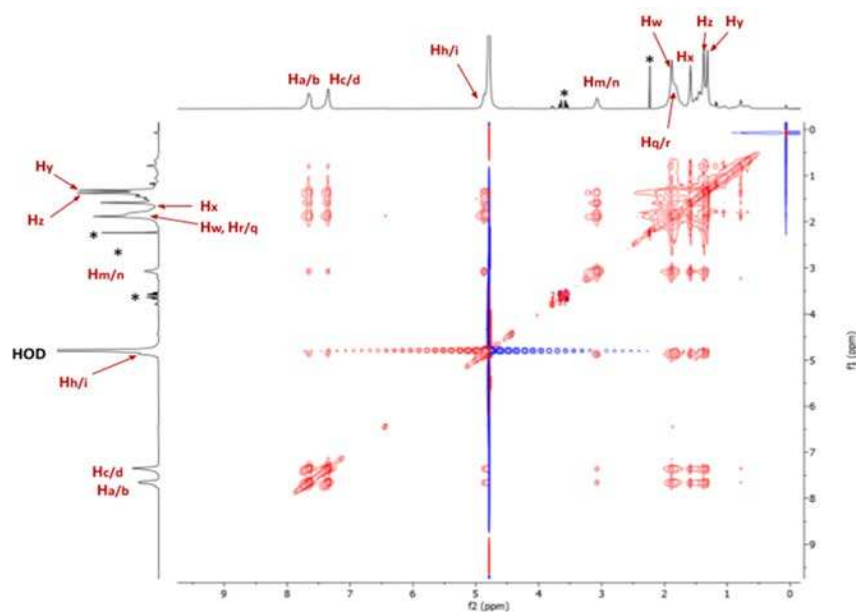


Figure 20: ^1H - ^1H NOESY NMR spectrum of 39 mM MK-2 in D_2O at 25°C. Asterisks (*) represent solvent impurities.

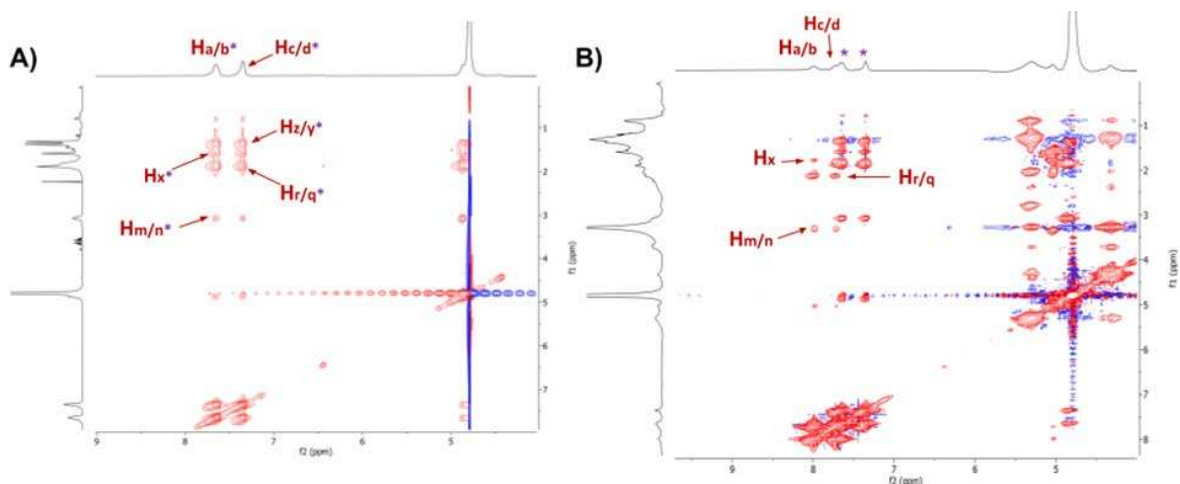


Figure 21: A) Partial 1H - 1H 2D NOESY NMR spectrum of 39 mM MK-2 in D_2O at 25°C. B) Partial 1H - 1H 2D NOESY NMR spectrum of 39 mM MK-2 incorporated into liposomes at 25°C. Comparison of spectral pattern, NOE strength, and relative chemical shift indicate that MK-2 resides in two distinct chemical environments in liposomal samples with relatively high concentrations of MK-2. Purple asterisks (*) represent peaks corresponding to MK-2 molecules interacting with aqueous solvent.

The NOE signals between the aromatic protons and $H_{r/q}$ have the highest intensity, whereas weak signals are observed between the aromatic protons and $H_{h/i}$. These NOE interactions suggest several possibilities regarding the conformation of MK-2 in aqueous solution: 1) the molecule is folded into a U-shaped conformation, similarly to what has been reported within a phospholipid monolayer environment, or 2) hydrophobic collapse of the isoprene chain. The latter possibility would be driven by thermodynamic effects, in which the alkyl chain is rearranged to minimize energetically unfavorable interactions with the polar solvent. In addition, it is possible that π interactions are occurring which further stabilize the observed conformation (Rich et al., 2003; Trembleau et al., 2003).

4.7 Inversion Recovery 1H NMR Spectroscopic Experiments: To further investigate interactions of MK-2 with the phospholipid bilayer, inversion recovery experiments were performed and T_1 relaxation times of several MK-2 and EPC protons were estimated at different ratios of MK-2 : lipid. Control experiments were performed using 39 mM MK-2

in D₂O (Figure 22). T₁ values were obtained for the aromatic MK-2 signals Ha/b and Hc/d (Figure 22), as these signals were well-resolved in aqueous solution and lacked spectral overlap with other known MK-2 signals that would influence the acquired integration values. The T₁ values for these signals were within 0.96 ± 0.02 s. A T₁ relaxation time of ~1.0 s for ¹H nuclei in small molecules is consistent with literature (Čuperlović-Culf, 2013), and subsequently our results for the control MK-2 sample validated the pulse delay sequence range utilized for further MK-2 inversion recovery experiments. In steady-state conditions, NMR peak width at half height $\Delta\nu_{1/2}$ and signal lifetime have a reciprocal relationship. Signal lifetime is dependent T₁ and T₂ relaxation time, and the following relationship is observed: $\Delta\nu_{1/2} = \frac{1}{\pi T_2}$ (Čuperlović-Culf, 2013). T₁ was considered to approximate T₂ in our MK-2 studies. Changes in $\Delta\nu_{1/2}$ and relaxation time are correlated with changes in intermolecular interactions (i.e., increased environmental viscosity, intermolecular binding) (Čuperlović-Culf, 2013; Nelson et al., 1987). In this work, these relationships between $\Delta\nu_{1/2}$ and relaxation rate were used to study the properties of MK-2 within a liposomal system.

To measure the T₁ relaxation for a system with a single membrane-bound population of MK-2, a liposome sample containing 16 mM MK-2 was implemented. This concentration was used because a 16 mM concentration consistently showed a single set of MK-2 peaks with a chemical shift consistent with bilayer interactions. Association of MK-2 with the membrane was verified by obtaining a 1D ¹H NMR spectrum of the liposomal 16 mM MK-2 sample. The presence of a single population of MK-2 that was incorporated into the bilayer was verified by comparison of chemical shift relative to the control (Table S2).

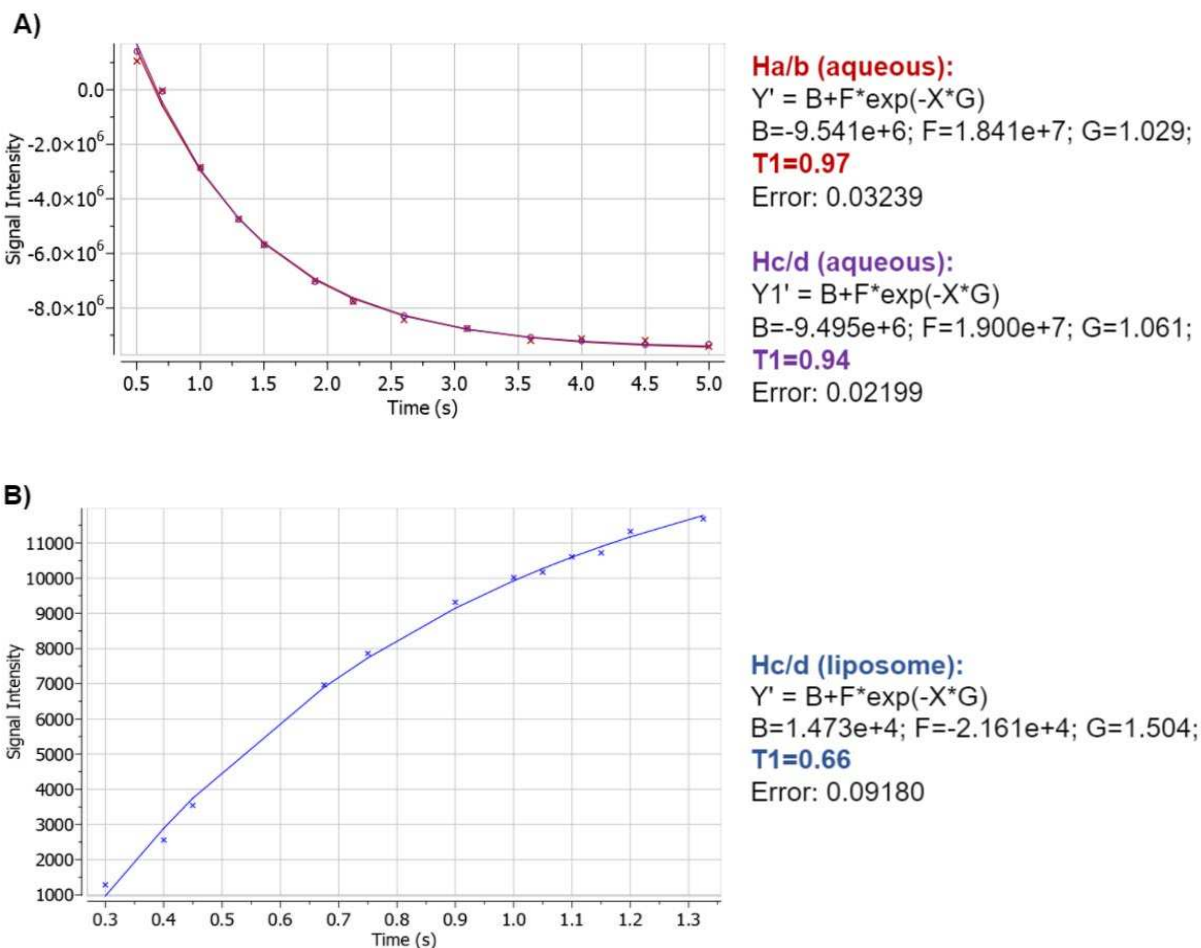


Figure 22: Comparison of T_1 relaxation time dependent on chemical environment. A) T_1 values for aromatic signals in an aqueous control spectrum of 39 mM MK-2. B) represents T_1 values for membrane-associated aromatic signals in a liposomal spectrum of 16 mM MK-2. T_1 lifetimes of MK-2 in liposomes are indirectly proportional to peak linewidth, suggesting changes in intermolecular interactions relative to the aqueous control sample.

The subsequent inversion recovery experiment showed line broadening and T_1 shortening for the aromatic peak Hc/d (Figure 19, Table S2). In the liposomal 16 mM MK-2 sample, the disproportionate change in relaxation time when compared to the change in linewidth may indicate chemical exchange. Since the protons on the aromatic ring of MK-2 are non-exchangeable, chemical exchange could occur due to exchange between the liposomal and aqueous subspecies of MK-2; i.e. the two species are associating and dissociating with the membrane interchangeably. A variable

temperature experiment was performed in order to probe the possibility of exchange (Figure S3 Appendices). The distance between signals and linewidth of both aqueous and liposomal $H_{a/b}$ and $H_{c/d}$ peaks were measured. However, these signals did not display significant coalescence. Subsequently, exchange was not measured in the variable temperature experiment, and if exchange of the two MK-2 populations is occurring, it is likely on a slower timescale. In future experiments, exchange spectroscopy (EXSY) NMR spectroscopic studies may be performed to further investigate the possibility of exchange.

4.8 Molecular Mechanics Simulations: ChemBio 3D was used to create a visual representation of the MK-2 structure indicated by our 2D NOESY NMR studies. Inter-proton distances determined using ChemBio 3D indicate that, in a MK-2 molecule with an extended isoprene chain, the shortest inter-proton distance between the most distant protons of the aromatic region ($H_{a/b}$) and the isoprenyl chain (H_m) is 7.4 Å. NOEs between $H_{a/b}$ and multiple isoprenyl protons suggest that MK-2 assumes a folded conformation in both aqueous and liposomal environments.

The basic 3D conformation indicated by NOE analysis is consistent with the U-shape illustrated for MK-2 in other model membranes (Koehn et al., 2018). However, the conformation of MK-2 within aqueous solution and at the phospholipid interface of the liposomes is indicated to be more tightly folded due to the presence of distinct NOE signals between the aromatic ring, the isoprenyl protons (H_x , $H_{r/q}$), and the terminal methyl groups (H_z , H_y) (Figures 14, 16, 17, 19, 20, 21). As a result, the mentioned isoprenyl protons were placed within 5 Å of $H_{a/b}$ and $H_{c/d}$ in our model. The ChemBio 3D representation was adjusted to reflect the NOE data from the 39 mM aqueous

spectrum (Figure 20) and 36 mM MK-2 NOESY spectrum in liposomes (Figure S2 Appendices), which suggest that H_x and H_y are equidistant from the aromatic ring. Future analysis will include conducting MMFF94 calculations on the structure in Figure 23, in order to obtain an energetically optimized structure.

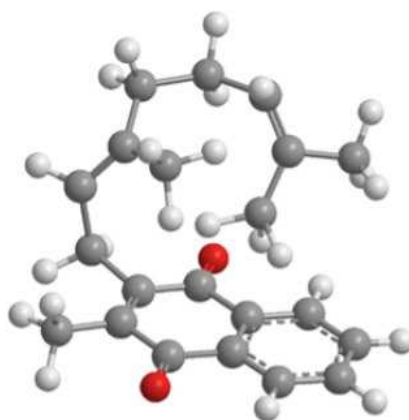


Figure 23: Illustration of MK-2 conformation in aqueous solution and upon interaction with EPC liposomes, as indicated by 2D ¹H-¹H NOESY NMR data. Molecular model created using ChemBio 3D 16.0. MM2 energy minimization was applied to all bond angles. The MK-2 conformation shown is not geometrically optimized.

Chapter 5 - Conclusions

Our laboratory has previously investigated the conformation of truncated quinone derivatives in multiple chemical environments (Koehn et al., 2018). The conformation of MK-2 has been characterized in systems that have been conventionally established as membrane mimetics, such as organic solvents with various dielectric constants, and phospholipid monolayers. While these model systems are simplified compared to the native membrane environment, they are considered useful for providing fundamental information regarding the properties of hydrophobic molecules that are challenging to study through both *in vitro* and *in vivo* experiments (Fuglestad et al., 2019; Mineev et al., 2016; Wand et al., 1998). With respect to preceding NMR-based studies by our laboratory, the utilization of a phospholipid monolayer in this study adds an additional degree of biological applicability.

In biological systems, MK molecules interact with ETS proteins buried within the phospholipid bilayer. It was therefore hypothesized that, in our study, MK-2 would be buried within the hydrophobic tails of the phospholipids. This prediction was supported by the previous research by our laboratory regarding the location of MK-2 in a monolayer system, in which it was concluded that MK-2 maintains interactions with both the polar head groups near the water pool and the proximal region of the surfactant tails (Koehn et al., 2018). Within the liposomal system used in this work, we observed evidence of MK-2 interactions with both the TMA region of the phospholipid head group and the allylic region of the EPC tails. Changes in chemical shift indicate that MK-2 resides in a more electronegative environment upon association with EPC liposomes,

suggesting that MK-2 largely interacts with the zwitterionic head group. The liposomal TMA signal interacts with both MK-2 aromatic protons $H_{a/b}$ and terminal methyl protons (H_z , H_y). Comprehensively, this indicates that the mid-isoprenyl region associates with the phospholipid tails, while the aromatic and terminal methyl protons interact with the zwitterionic head groups of the bilayer. To further verify that MK-2 is incorporated into the model membrane, paramagnetic relaxation enhancement (PRE) techniques will be implemented, in which a paramagnetic probe is added to the bulk D_2O solvent of the liposomal system. Relaxation time shortening and peak broadening of the MK signals would indicate that MK interacts with the solvent, whereas non-significant changes in these parameters would support the interpretation that the putative liposomal population of MK-2 is embedded in the bilayer.

MK-2 is sparingly more polar than native MK molecules due to its shortened isoprene chain. Subsequently, the reduced hydrophobicity of MK-2 and folding of its side chain may cause localization near the phospholipid head groups at the water interface to be more energetically favorable than exclusive interactions with the phospholipid tails. It is possible that the MK location determined using our truncated derivative is not physiologically representative, given the high hydrophobicity of native MK molecules with long isoprene chains. However, our findings suggest that the differing properties of the naphthoquinone and isoprene moieties of MK are important not only for protein binding events, but also dictate the location of MK molecules within the quinone pool. Identification of factors that influence MK conformation and location may improve understanding of MK diffusion and localization within the bilayer. Experimental data is critical for validating computational studies that investigate quinone dynamics, and may

contribute to studies relevant toward targeting the prokaryotic electron transport chain to combat antibiotic resistance.

Analysis of the NOESY spectra at 19 mM, 36 mM, and 39 mM MK-2 supports the interpretation that two populations of MK-2 are present at higher concentrations. One population is presumably in a membrane-bound environment, and the other is believed to be located at the aqueous interface of the phospholipid head groups. The results of this study indicate that incorporation of MK-2 into the phospholipid bilayer occurs as a function of concentration. At lower concentrations of MK-2 relative to the liposomes, complete association of the MK-2 population with the bilayer was observed. As the concentration of MK-2 increased, additional NMR signals emerged that were consistent with the formation of an aqueous population of MK-2. The formation of two subspecies of MK-2 in this study was likely an oversaturation effect resulting from experimental factors. For the NMR spectroscopic experiments, it was necessary to use relatively large concentrations of MK-2 and small liposomes (100 nm) to produce spectra with sufficient resolution. Native cell membranes are appreciably larger in diameter; this increased surface area would likely enable incorporation of greater amounts of MK-2 into the bilayer. Therefore, use of larger vesicles or a lipid constituent with different packing properties/curvature may influence formation of this aqueous subspecies. In studies of related quinone molecules such as ubiquinone (UBQ), it was reported that a ratio $\leq 1 : 50$ of UBQ : phospholipid was physiologically equivalent (Lenaz, 1988; Samori et al., 1992). It is possible that similar ratios of quinone to lipid are present in MK-utilizing organisms. Together, these factors suggest that the emergence of an aqueous subspecies of MK-2 is not a physiologically relevant phenomenon. As described in Chapter 2, several methods of sample preparation

were attempted to maximize MK-2 incorporation into the bilayer. The most effective method was identified and utilized for subsequent NMR experiments. Although it is possible that additional troubleshooting could decrease formation of the aqueous MK-2 subspecies, further method development in this area was not pursued for our objectives, since enough liposome-associated MK-2 was obtained by our methods to study its basic intermolecular and intramolecular properties.

1D ^1H and 2D ^1H - ^1H NMR data from this work indicate that MK-2 assumes a folded conformation upon association with an L- α -phosphatidylcholine (EPC) bilayer. This finding is consistent with previous studies by our lab, which indicate that MK-2 assumes a U-shaped conformation in both organic solvent and reverse micelle lipid monolayers (Koehn et al., 2018). Our data shows NOEs between the aromatic protons and isoprene protons of MK-2 in both D_2O and EPC liposomes. These NOE interactions are absent in all 2D MK-2 spectra from the preceding publication, regardless of solvent and surfactant environment. This may be attributed to factors independent of inter-proton distances, since NOE signal strength is dependent on many factors including solvent viscosity, molecular size (Edison et al., 2010), and instrument parameters. Alternatively, the appearance of the additional NOEs may represent true conformational differences, in which naphthoquinone head group and isoprene chain are in closer proximity. The strength of the NOE signals suggests that MK-2 assumes a tightly folded structure in both aqueous solution and EPC liposomes, in which the through-space distance between the aromatic ring and terminal methyl groups is less than 4 Å. If the proposed structure is accurate, it is most likely driven by hydrophobic effects, and possibly π interactions between the MK-2 isoprene chain and aromatic ring. The work presented

herein is consistent with previous studies that use NMR to determine the 3D conformation of MK-2.

2D NOESY spectroscopic analysis indicates that MK-2 assumes a similar folded conformation in both aqueous solution and within the phospholipid head group region of the liposome. It was previously concluded by our laboratory that a folded conformation of MK-2 is maintained in both aprotic and hydrophobic environments. It was also determined that the degree of folding and precise steric arrangement varies depending on the polarity/hydrophobicity of the chemical environment (Koehn et al., 2018). In the work presented herein, the NOESY data did not indicate appreciable differences in MK-2 conformation in aqueous solution or upon association with the polar heads of the liposomes. However, this may be attributed to the charged nature of the phospholipid head groups, since the folded conformation of MK-2 in aqueous solution is likely favorable in more polar environments as well. Although NOE interactions from this study provide preliminary evidence of MK-2 interaction with the allylic region of the phospholipids, further analysis is needed to confirm this possibility. In any case, the folded conformation and reduced hydrophobicity of the truncated isoprene chain likely result in both the naphthoquinone and alkyl moieties residing more closely to the more polar environment of the phospholipid head groups.

A limitation of the membrane model used for this work is its implementation of the mammalian phospholipid EPC to study MK in the context of bacterial electron transport. Therefore, subsequent studies will implement 16:0 phosphatidylglycerol, an anionic lipid that forms liposome bilayers (Kalra & Bally, 2013) and is structurally similar to phosphatidylglycerol derivatives that are abundant in pathogen plasma membranes

(Sohlenkamp et al., 2016). It is possible that the negatively charged head group and fully saturated tail region will significantly affect the location of the truncated MK-2 molecules used by our laboratory. However, it is important to consider that native bacterial membranes are heterogenous and composed of various lipids with differing charges (Erand et al., 2009). Once basic systems using model membranes with single-lipid components have been characterized, it may be useful to study MK-liposome interactions using more complex and physiologically representative lipid formulations. The manner in which lipid composition may dictate MK interactions with the plasma membrane requires further investigation.

As mentioned previously, much of what is known regarding MK conformation has been derived from computational experiments. Therefore, obtaining experimental evidence to complement these *in silico* studies may be instrumental for elucidating the relationship between MK structure, conformation, redox activity, and membrane diffusion. To this end, MK-2 was used in this study for preliminary characterization of MK conformation. However, the folded conformation determined in this manuscript may not be representative of native MK configurations, since the properties of MK-2 differ with respect to biological MK derivatives due to its truncated isoprene chain. NMR-based determination of the conformation of native MK derivatives is challenging due to the likelihood of spectral overlap between isoprene protons residing in similar chemical environments. However, knowledge regarding MK spectral pattern and properties obtained in the work herein will provide reference data for studies of MK derivatives with longer isoprene chains. Our findings support previous work in our laboratory (Koehn et al. 2018) indicating that MK-2 configurations differing from the all-*trans* MK

conformations depicted in literature are assumed in different chemical environments. It is possible that folded or *gauche* conformations are relevant to biologically active MK derivatives as well, which requires further examination using longer MK variants.

In future studies, examining the effects of naphthoquinone redox state on MK folding may be useful for assessing the biological relevance of changes in MK conformation.

For example, potential differences in MK folding upon reduction of the carbonyl groups may have important implications for MK binding with ETS electron donor proteins versus terminal electron acceptors. Differences in MK conformation depending on its redox state may affect preferential binding to either complex, which would facilitate understanding of kinetic regulation of the quinone pool within prokaryotic electron transport systems.

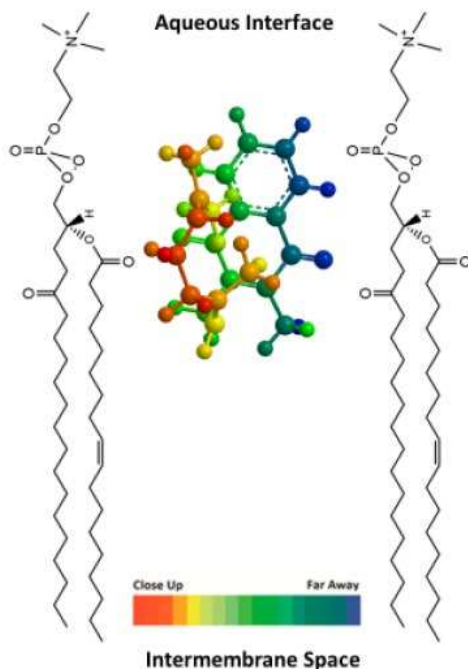


Figure 24: Schematic representing the location and conformation of MK-2 within an L- α -phosphatidylcholine (EPC) liposomal bilayer, as determined by 1D ^1H and 2D ^1H - ^1H spectroscopic analysis. Molecular model was created using Chem3D 16.0; EPC structure was created using ChemDraw Professional 16.0.

References

- Anglister, J., Srivastava, G., & Naider, F. (2016). Detection of intermolecular NOE interactions in large protein complexes. *Progress in nuclear magnetic resonance spectroscopy*, 97, 40–56. <https://doi.org/10.1016/j.pnmrs.2016.08.002>
- Arsene, M.-L., Răut, I., Călin, M., Jecu, M.-L., Doni, M., & Gurban, A.-M. (2021). Versatility of Reverse Micelles: From Biomimetic Models to Nano (Bio)Sensor Design. *Processes*, 9(2), 345. doi:10.3390/pr9020345
- Avanti Polar Lipids (2021, May 18). How Should I Store My Liposomes? *Avanti Polar Lipids*. <https://avantilipids.com/tech-support/faqs/liposome-storage>
- Avanti Polar Lipids (2021, May 18). Preparing Large, Unilamellar Vesicles by Extrusion (LUVET). *Avanti Polar Lipids*. <https://avantilipids.com/tech-support/liposome-preparation/luvet>
- Baker, R. P., & Urban, S. (2017). An Inducible Reconstitution System for the Real-Time Kinetic Analysis of Protease Activity and Inhibition Inside the Membrane. *Methods in enzymology*, 584, 229–253. <https://doi.org/10.1016/bs.mie.2016.10.025>
- Bashiri, G., Nigon, L. V., Jirgis, E., Ho, N., Stanborough, T., Dawes, S. S., Baker, E. N., Bulloch, E., & Johnston, J. M. (2020). Allosteric regulation of menaquinone (vitamin K2) biosynthesis in the human pathogen *Mycobacterium tuberculosis*. *The Journal of biological chemistry*, 295(12), 3759–3770.

<https://doi.org/10.1074/jbc.RA119.012158>

Blaza, J. N., Bridges, H. R., Aragão, D., Dunn, E. A., Heikal, A., Cook, G. M., Nakatani, Y., & Hirst, J. (2017). The mechanism of catalysis by type-II NADH:quinone oxidoreductases. *Scientific reports*, 7, 40165. <https://doi.org/10.1038/srep40165>

Boersch, M., Rudrawar, S., Grant, G., & Zunk, M. (2018). Menaquinone biosynthesis inhibition: a review of advancements toward a new antibiotic mechanism. *RSC Advances*, 8, 5099-5105. <https://doi.org/10.1039/C7RA12950E>

Bublitz, G. R., Doucette, K.A., Crans, D.C. (2020). ¹H NMR Study of Menaquinone-2 Interactions in a Phosphatidylcholine Liposome Membrane Model. *American Chemical Society Rocky Mountain Regional Meeting, 2020*. Abstract and Presentation 77.

Burgess, S. (1998). Liposome Preparation – Avanti Polar Lipids. Retrieved May 18, 2021 from <https://www.sigmaaldrich.com/US/en/technical-documents/protocol/cell-culture-and-cell-culture-analysis/transfection-and-gene-editing/liposome-preparation>

Cardia, M.C., Caddeo, C., Lai, F., Fadda, A., Sinico, C., & Luhmer, M. (2019). ¹H NMR study of the interaction of trans-resveratrol with soybean phosphatidylcholine liposomes. *Sci. Rep.* 9, 17736. <https://doi.org/10.1038/s41598-019-54199-7>

Casares, D., Escribá, P. V., & Rosselló, C. A. (2019). Membrane Lipid Composition: Effect on Membrane and Organelle Structure, Function and Compartmentalization and Therapeutic Avenues. *International journal of molecular sciences*, 20(9), 2167. <https://doi.org/10.3390/ijms20092167>

- Cho, G., Lee, E. & Kim, J (2021). Structural insights into phosphatidylethanolamine formation in bacterial membrane biogenesis. *Sci. Rep.* *11*, 5785
<https://doi.org/10.1038/s41598-021-85195-5>
- Choi, S. R., Frandsen, J., & Narayanasamy, P. (2017). Novel long-chain compounds with both immunomodulatory and MenA inhibitory activities against *Staphylococcus aureus* and its biofilm. *Scientific Reports*, *7*, 40077.
<https://doi.org/10.1038/srep40077>
- Clore, G. (2015). NMR in structural and cell biology. *Encyclopedia of Cell Biology*, *1*, 98-107. <https://doi.org/10.1016/B978-0-12-394447-4.10019-7>
- Čuperlović-Culf, M. (2013). NMR Metabolomics in Cancer Research. *Woodhead Publishing Series in Biomedicine*, 139-213.
<https://doi.org/10.1533/9781908818263.139>
- Doucette, K.A. (2021). *The Use of Model Membrane Techniques for the Analysis of Interactions, Conformation, and Redox Properties of Menaquinones and Other Small Molecules*. [Doctoral dissertation, Colorado State University].
<https://hdl.handle.net/10217/232560>
- Drazenovic, J., Wang, H., Roth, K., Zhang, J., Ahmed, S., Chen, Y., Bothun, G., & Wunder, S. L. (2015). Effect of lamellarity and size on calorimetric phase transitions in single component phosphatidylcholine vesicles. *Biochimica et biophysica acta*, *1848*(2), 532–543.
<https://doi.org/10.1016/j.bbamem.2014.10.003>
- Edison, A.S., Schroeder, F.C. (2010). NMR – Small Molecules and Analysis of Complex

Mixtures. *Comprehensive Natural Products II. Elsevier*, 169-196.

<https://doi.org/10.1016/B978-008045382-8.00196-9>.

Epand, R. M., & Epand, R. F. (2009). Lipid domains in bacterial membranes and the action of antimicrobial agents. *Biochimica et biophysica acta*, 1788(1), 289–294.
<https://doi.org/10.1016/j.bbamem.2008.08.023>

Fritsch, V. N., Loi, V. V., Busche, T., Sommer, A., Tedin, K., Nürnberg, D. J., Kalinowski, J., Bernhardt, J., Fulde, M., & Antelmann, H. (2019). The MarR-Type Repressor MhqR Confers Quinone and Antimicrobial Resistance in *Staphylococcus aureus*. *Antioxidants & redox signaling*, 31(16), 1235–1252.
<https://doi.org/10.1089/ars.2019.7750>

Fuglestad, B., Marques, B. S., Jorge, C., Kerstetter, N. E., Valentine, K. G., & Wand, A.J. (2019). Reverse Micelle Encapsulation of Proteins for NMR Spectroscopy. *Methods in enzymology*, 615, 43–75. <https://doi.org/10.1016/bs.mie.2018.08.032>

Fowler, S., Roush, R., & Wise, J. (2013). *Concepts of Biology*. Houston, TX: OpenStax. Retrieved May 18, 2021 from <https://openstax.org/books/concepts-biology/pages/3-2-comparing-prokaryotic-and-eukaryotic-cells>

Grimaldi, N., Andrade, F., Segovia, N., Ferrer-Tasies, L., Sala, S., Veciana, J., & Ventosa, N. (2016). Lipid-based nanovesicles for nanomedicine. *Chemical Society Reviews*, 45(23), 6520–6545. <https://doi.org/10.1039/c6cs00409a>

Grimaldi, S., Arias-Cartin, R., Lanciano, P., Lyubenova, S., Szenes, R., Endeward, B., Prisner, T., Guigliarelli, B., & Magalon, A. (2012). Determination of the Proton Environment of High Stability Menasemiquinone Intermediate in *Escherichia coli*

- Nitrate Reductase A by Pulsed EPR*. *The Journal of Biological Chemistry*, 287, 4662 - 4670. <https://doi.org/10.1074/jbc.M111.325100>
- Guan, H. H., Hsieh, Y. C., Lin, P. J., Huang, Y. C., Yoshimura, M., Chen, L. Y., Chen, S. K., Chuankhayan, P., Lin, C. C., Chen, N. C., Nakagawa, A., Chan, S. I., & Chen, C. J. (2018). Structural insights into the electron/proton transfer pathways in the quinol:fumarate reductase from *Desulfovibrio gigas*. *Scientific Reports*, 8(1), 14935. <https://doi.org/10.1038/s41598-018-33193-5>
- Guin, P.S., Das, S., & Mandal, P. (2011). Electrochemical Reduction of Quinones in Different Media: A Review. *International journal of electrochemistry*, 2011, 1-22. <https://doi.org/10.4061/2011/816202>
- Hayashi, J. M., & Morita, Y. S. (2019). Mycobacterial Membrane Domain, or a Primordial Organelle?. *The Yale journal of biology and medicine*, 92(3), 549–556.
- Johnston, J. M., & Bulloch, E. M. (2020). Advances in menaquinone biosynthesis: sublocalisation and allosteric regulation. *Current opinion in structural biology*, 65, 33–41. <https://doi.org/10.1016/j.sbi.2020.05.005>
- Hiratsuka, T., Furihata, K., Ishikawa, J., Yamashita, H., Itoh, N., Seto, H., & Dairi, T. (2008). An alternative menaquinone biosynthetic pathway operating in microorganisms. *Science (New York, N.Y.)*, 321(5896), 1670–1673. <https://doi.org/10.1126/science.1160446>
- Joshi, S., Fedoseyenko, D., Mahanta, N., Manion, H., Naseem, S., Dairi, T., & Begley, T. P. (2018). Novel enzymology in futasosine-dependent menaquinone

biosynthesis. *Current opinion in chemical biology*, 47, 134–141.

<https://doi.org/10.1016/j.cbpa.2018.09.015>

Kalra J., Bally M.B. (2013) Liposomes. In: Uchegbu I., Schätzlein A., Cheng W., Lalatsa A. *Fundamentals of Pharmaceutical Nanoscience*. Springer, 27-63.

https://doi.org/10.1007/978-1-4614-9164-4_3

Ko, Y. H., Kim, Y., Kim, H., & Kim, K. (2011). U-shaped conformation of alkyl chains bound to a synthetic receptor cucurbit[8]uril. *Chemistry, an Asian journal*, 6(2), 652–657. <https://doi.org/10.1002/asia.201000665>

Krueger, F. R., Werther, W., Kissel, J., & Schmid, E. R. (2004). Assignment of quinone derivatives as the main compound class composing 'interstellar' grains based on both polarity ions detected by the 'Cometary and Interstellar Dust Analyser' (CIDA) onboard the spacecraft STARDUST. *Rapid communications in mass spectrometry : RCM*, 18(1), 103–111. <https://doi.org/10.1002/rcm.1291>

Kurosu, M., & Begari, E. (2010). Vitamin K2 in electron transport system: are enzymes involved in vitamin K2 biosynthesis promising drug targets?. *Molecules (Basel, Switzerland)*, 15(3), 1531–1553. <https://doi.org/10.3390/molecules15031531>

Kumar, S., Koehn, J. T., Gonzalez-Juarrero, M., Crans, D. C., & Crick, D. C. (2020). Mycobacterium tuberculosis Survival in J774A.1 Cells Is Dependent on MenJ Moonlighting Activity, Not Its Enzymatic Activity. *ACS Infectious Diseases*, 6(10), 2661–2671. <https://doi.org/10.1021/acsinfecdis.0c00312>

Lenaz, G., Fato, R., Formiggini, G., & Genova, M. L. (2007). The role of Coenzyme Q in

- mitochondrial electron transport. *Mitochondrion*, 7 Suppl, S8–S33.
<https://doi.org/10.1016/j.mito.2007.03.009>
- Lenaz, G. Role of mobility of redox components in the inner mitochondrial membrane. *J. Membrin Biol.* 104, 193–209 (1988). <https://doi.org/10.1007/BF01872322>
- Liang, B., & Tamm, L. K. (2016). NMR as a tool to investigate the structure, dynamics and function of membrane proteins. *Nature Structural & Molecular Biology*, 23(6), 468– 474. <https://doi.org/10.1038/nsmb.3226>
- Lu, X., Zhang, H., Tonge, P. J., & Tan, D. S. (2008). Mechanism-based inhibitors of MenE, an acyl-CoA synthetase involved in bacterial menaquinone biosynthesis. *Bioorganic & Medicinal Chemistry Letters*, 18(22), 5963–5966.
<https://doi.org/10.1016/j.bmcl.2008.07.130>
- Marion D. (2013). An introduction to biological NMR spectroscopy. *Molecular & cellular proteomics : MCP*, 12(11), 3006–3025. <https://doi.org/10.1074/mcp.O113.030239>
- Mineev, K. & Nadezhdin, K. (2017). Membrane mimetics for solution NMR studies of membrane proteins. *Nanotechnology Reviews*, 6(1), 15-32.
<https://doi.org/10.1515/ntrev-2016-0074>
- Nakatani, Y., Shimaki, Y., Dutta, D., Muench, S. P., Ireton, K., Cook, G. M., & Jeuken, L. (2020). Unprecedented Properties of Phenothiazines Unraveled by a NDH-2 Bioelectrochemical Assay Platform. *Journal of the American Chemical Society*, 142(3), 1311–1320. <https://doi.org/10.1021/jacs.9b10254>
- Nelson, T.R., Tung S.M. (1987). Temperature dependence of proton relaxation times in

vitro. *Magn Reson Imaging*. 5(3):189-99.

[https://doi.org/10.1016/0730-725X\(87\)90020-8](https://doi.org/10.1016/0730-725X(87)90020-8)

Nowicka, B., & Kruk, J. (2010). Occurrence, biosynthesis and function of isoprenoid quinones. *Biochimica et Biophysica Acta*, 1797(9), 1587–1605.

<https://doi.org/10.1016/j.bbabi.2010.06.007>

Panthee, S., Paudel, A., Hamamoto, H., Uhlemann, A. C., & Sekimizu, K. (2020). The Role of Amino Acid Substitution in HepT Toward Menaquinone Isoprenoid Chain Length Definition and Lysocin E Sensitivity in *Staphylococcus aureus*. *Frontiers in Microbiology*, 11, 2076. <https://doi.org/10.3389/fmicb.2020.02076>

Paudel, A., Hamamoto, H., Panthee, S., & Sekimizu, K. (2016). Menaquinone as a potential target of antibacterial agents. *Drug Discoveries & Therapeutics*, 10(3), 123–128. <https://doi.org/10.5582/ddt.2016.01041>

Peters, B. J., Van Cleave, C., Haase, A. A., Hough, J., Giffen-Kent, K. A., Cardiff, G. M., Sostarecz, A. G., Crick, D. C., & Crans, D. C. (2018). Structure Dependence of Pyridine and Benzene Derivatives on Interactions with Model Membranes.

Langmuir : The ACS Journal of Surfaces and Colloids, 34(30), 8939–8951.

<https://doi.org/10.1021/acs.langmuir.8b01661>

Peters, B. J., Groninger, A. S., Fontes, F. L., Crick, D. C., & Crans, D. C. (2016). Differences in Interactions of Benzoic Acid and Benzoate with Interfaces.

Langmuir: The ACS Journal of Surfaces and Colloids, 32(37), 9451-9459.

<https://doi.org/10.1021/acs.langmuir.6b02073>

Puffal, J., Mayfield, J. A., Moody, D. B., & Morita, Y. S. (2018). Demethylmenaquinone

- Methyl Transferase Is a Membrane Domain-Associated Protein Essential for Menaquinone Homeostasis in *Mycobacterium smegmatis*. *Frontiers in microbiology*, 9, 3145. <https://doi.org/10.3389/fmicb.2018.03145>
- Ramos, A. P., Cruz, M., Tovani, C. B., & Ciancaglini, P. (2017). Biomedical applications of nanotechnology. *Biophysical reviews*, 9(2), 79–89. <https://doi.org/10.1007/s12551-016-0246-2>
- Rich, D., Estiarte, M.A., & Philip, A. (2003). Stereochemical Aspects of Drug Action I: Conformational Restriction, Steric Hindrance, and Hydrophobic Collapse. *The Practice of Medicinal Chemistry*, 373-386. <https://doi.org/10.1016/B978-012744481-9/50027-1>
- Rosales-Mendoza S., González-Ortega O. (2019) Liposome-Based Nanovaccines. In: Nanovaccines. *Springer, Cham.*, 233-265. https://doi.org/10.1007/978-3-030-31668-6_9
- Rubinson, K. A., Practical corrections for p(H,D) measurements in mixed H₂O/D₂O biological buffers. *Analytical Methods* 2017, 9 (18), 2744-2750.
- Samorì, B., Lenaz, G., Battino, M., Marconi, G., & Domini, I. (1992). On coenzyme Q orientation in membranes: a linear dichroism study of ubiquinones in a model bilayer. *The Journal of Membrane Biology*, 128(3), 193–203. <https://doi.org/10.1007/BF00231812>
- Schurig-Briccio, L. A., Yano, T., Rubin, H., & Gennis, R. B. (2014). Characterization of the type 2 NADH:menaquinone oxidoreductases from *Staphylococcus aureus*

- and the bactericidal action of phenothiazines. *Biochimica et biophysica acta*, 1837(7), 954–963. <https://doi.org/10.1016/j.bbabi.2014.03.017>
- Sebaaly, C., Greige-Gerges, H., & Charcosset, C. (2019). Lipid membrane models for Biomembrane Properties' Investigation. *Elsevier*, 311-340. <https://doi.org/10.1016/B978-0-12-813606-5.00011-7>.
- Seif Eddine, M., Biaso, F., Arias-Cartin, R., Pilet, E., Rendon, J., Lyubenova, S., Seduk, F., Guigliarelli, B., Magalon, A., & Grimaldi, S. (2017). Probing the Menasemiquinone Binding Mode to Nitrate Reductase A by Selective 2H and 15N Labeling, HYSCORE Spectroscopy, and DFT Modeling. *ChemPhysChem: a European journal of chemical physics and physical chemistry*, 18(19), 2704–2714. <https://doi.org/10.1002/cphc.201700571>
- Sellamuthu, S., Singh, M., Kumar, A., & Singh, S. K. (2017). Type-II NADH Dehydrogenase (NDH-2): a promising therapeutic target for antitubercular and antibacterial drug discovery. *Expert opinion on therapeutic targets*, 21(6), 559–570. <https://doi.org/10.1080/14728222.2017.1327577>
- Singharoy, A., Maffeo, C., Delgado-Magnero, K. H., Swainsbury, D., Sener, M., Kleinekathöfer, U., Vant, J. W., Nguyen, J., Hitchcock, A., Isralewitz, B., Teo, I., Chandler, D. E., Stone, J. E., Phillips, J. C., Pogorelov, T. V., Mallus, M. I., Chipot, C., Luthey-Schulten, Z., Tieleman, D. P., Hunter, C. N., ... Schulten, K. (2019). Atoms to Phenotypes: Molecular Design Principles of Cellular Energy Metabolism. *Cell*, 179(5), 1098–1111.e23. <https://doi.org/10.1016/j.cell.2019.10.021>

- Sohlenkamp, C., & Geiger, O. (2016). Bacterial membrane lipids: diversity in structures and pathways. *FEMS microbiology reviews*, 40(1), 133–159.
<https://doi.org/10.1093/femsre/fuv008>
- Thompson A.M., Denny W.A. (2019). Inhibitors of enzymes in the electron transport chain of *Mycobacterium tuberculosis*. *Reports in Medicinal Chemistry, Academic Press*, 52, 97-130. <https://doi.org/10.1016/bs.armc.2019.05.001>
- Trembleau L, Rebek J Jr. (2003). Helical conformation of alkanes in a hydrophobic cavitand. *Science*, 301(5637), 1219-1220. doi: 10.1126/science.1086644.
- Upadhyay A, Fontes FL, Gonzalez-Juarrero M, McNeil MR, Crans DC, Jackson M, Crick DC. Partial Saturation of Menaquinone in *Mycobacterium tuberculosis*: Function and Essentiality of a Novel Reductase, MenJ. *ACS Cent Sci.*, 1(6), 292-302. <https://doi.org/10.1021/acscentsci.5b00212>
- Van den Brink-Van der Laan, E., Killian, J. A., & de Kruijff, B. (2004). Nonbilayer lipids affect peripheral and integral membrane proteins via changes in the lateral pressure profile. *Biochimica et biophysica acta*, 1666(1-2), 275–288.
<https://doi.org/10.1016/j.bbamem.2004.06.010>
- Van der Veen, J. N., Kennelly, J. P., Wan, S., Vance, J. E., Vance, D. E., & Jacobs, R. L. (2017). The critical role of phosphatidylcholine and phosphatidylethanolamine metabolism in health and disease. *Biochimica et biophysica acta. Biomembranes*, 1859(9 Pt B), 1558–1572.
<https://doi.org/10.1016/j.bbamem.2017.04.006>
- Wand, A. J., Ehrhardt, M. R., & Flynn, P. F. (1998). High-resolution NMR of

encapsulated proteins dissolved in low-viscosity fluids. *Proceedings of the National Academy of Sciences of the United States of America*, 95(26), 15299–15302. <https://doi.org/10.1073/pnas.95.26.15299>

Warschawski, D. E., Arnold, A. A., Beaugrand, M., Gravel, A., Chartrand, É., & Marcotte, I. (2011). Choosing membrane mimetics for NMR structural studies of transmembrane proteins. *Biochimica et biophysica acta*, 1808(8), 1957–1974. <https://doi.org/10.1016/j.bbamem.2011.03.016>

Xu, J., Ding, Z., Liu, B., Yi, S.M., Li, J., Zhang, Z., Liu, Y., Liu, L., Zhou, A., Gennis, R., & Zhu, J. (2020). Structure of the cytochrome aa3-600 heme-copper menaquinol oxidase bound to inhibitor HQNO shows TM0 is part of the quinol binding site. *Proceedings of the National Academy of Sciences*, 117, 872 - 876. <https://doi.org/10.1073/pnas.1915013117>

Yano, T., Rahimian, M., Aneja, K. K., Schechter, N. M., Rubin, H., & Scott, C. P. (2014). Mycobacterium tuberculosis type II NADH-menaquinone oxidoreductase catalyzes electron transfer through a two-site ping-pong mechanism and has two quinone-binding sites. *Biochemistry*, 53(7), 1179–1190. <https://doi.org/10.1021/bi4013897>

Yeh, V., Goode, A., & Bonev, B. B. (2020). Membrane Protein Structure Determination and Characterisation by Solution and Solid-State NMR. *Biology*, 9(11), 396. [doi:10.3390/biology9110396](https://doi.org/10.3390/biology9110396)

Yi, S. M., Narasimhulu, K. V., Samoilova, R. I., Gennis, R. B., & Dikanov, S. A. (2010). Characterization of the semiquinone radical stabilized by the cytochrome aa3-

600 menaquinol oxidase of *Bacillus subtilis*. *The Journal of biological chemistry*, 285(24), 18241–18251. <https://doi.org/10.1074/jbc.M110.116186>

Zhang, Z., Liu, L., Liu, C. et al. (2021). New aspects of microbial vitamin K2 production by expanding the product spectrum. *Microb Cell Fact*, 20, 84. <https://doi.org/10.1186/s12934-021-01574-7>

Zhang H. (2017) Thin-Film Hydration Followed by Extrusion Method for Liposome Preparation. *Liposomes. Methods in Molecular Biology*, 1522, 17-22. https://doi.org/10.1007/978-1-4939-6591-5_2

Appendices

Table S1: Data obtained from DLS experiments to confirm the formation of unilamellar vesicles and to compare vesicle size at different ratios of MK-2 and lipid; total concentration equates to 100mg/mL per sample. Percentages were determined according to %w/w. Differences in mean particle size were not statistically significant. The DLS data shown is included in a collaborative manuscript (Doucette, 2021).

Sample	Size (d.nm)	Z-Average	Standard Deviation (d.nm)	Polydispersity Index
Control (blank liposomes, 100% EPC)	162.0	147.5	50.98	0.082
4% MK-2 96% EPC	153.1	138.2	47.66	0.091
6% MK-2 94% EPC	163.5	141.0	55.55	0.137
8% MK-2 92% EPC	173.8	147.0	67.38	0.145
12% MK-2 88% EPC	183.7	151.3	78.66	0.165

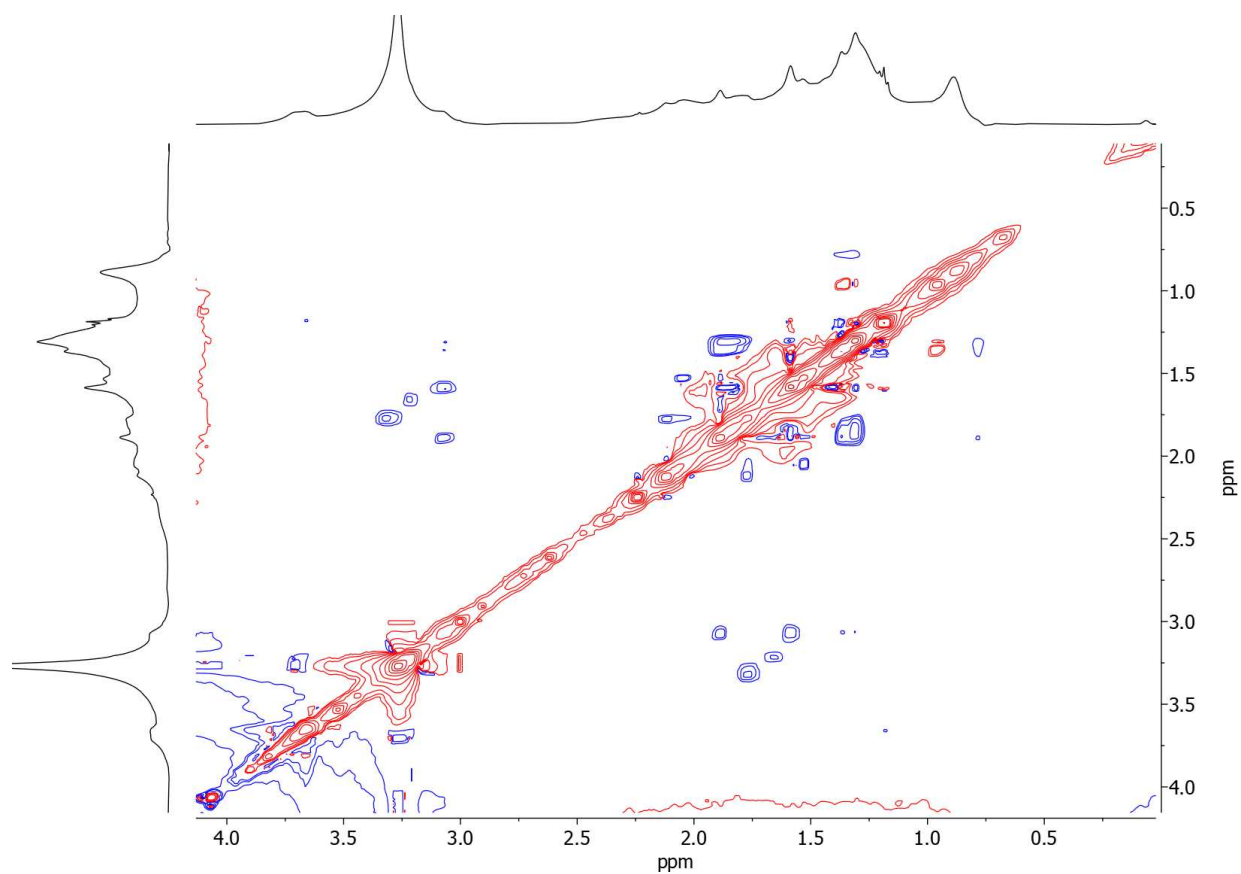


Figure S1: Partial ^1H - ^1H 2D ROESY NMR spectrum of 39 mM MK-2 in 130 mM EPC liposomes. Intramolecular NOE cross talk indicates through-space interactions between the distal isoprenyl protons and isoprenyl protons that are close in proximity to the naphthoquinone moiety. ROESY spectrum adapted with modification from a collaborative project (Doucette 2021).

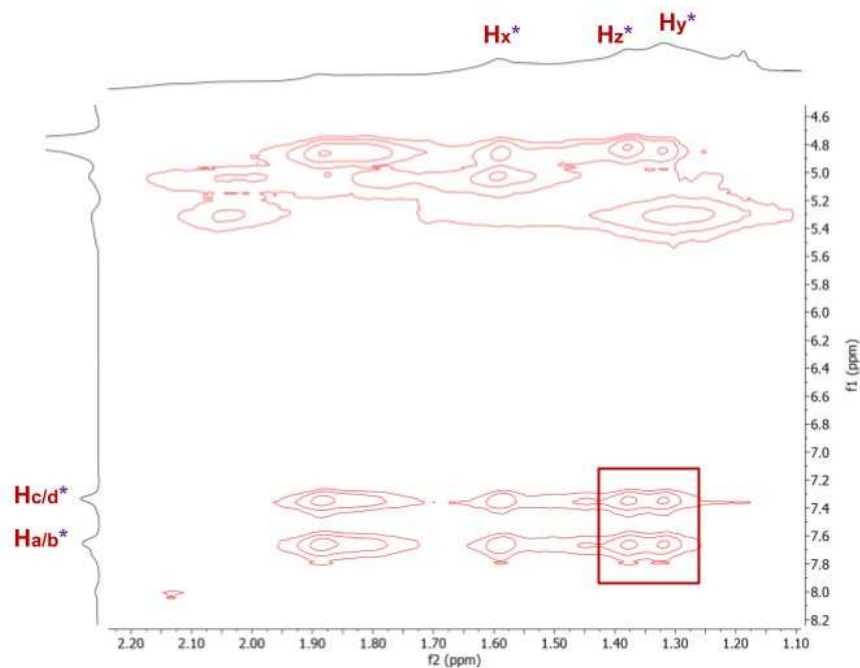


Figure S2: Partial ^1H - ^1H NOESY NMR spectrum of 36 mM MK-2 in 130 mM EPC liposomes at 25°C. Highlighted region (red) indicates resolved region of interactions of Hz and Hy with the aromatic protons Ha/b and Hc/d in an aqueous environment. Purple asterisks (*) represent peaks corresponding to MK-2 molecules interacting with aqueous solvent.

Table S2: Summary of chemical shift, linewidth at half-height ($\Delta\nu_{1/2}$), and T_1 relaxation time values for aromatic peak Hc/d in aqueous environments and upon association with liposomes.

Assignment	Chemical Shift (ppm)	$\Delta\nu_{1/2}$	T_1 (s)
39 mM (aqueous)	7.35	13.03	0.94 ± 0.02 s
16 mM (liposome)	7.68	29.56	0.66 ± 0.09 s

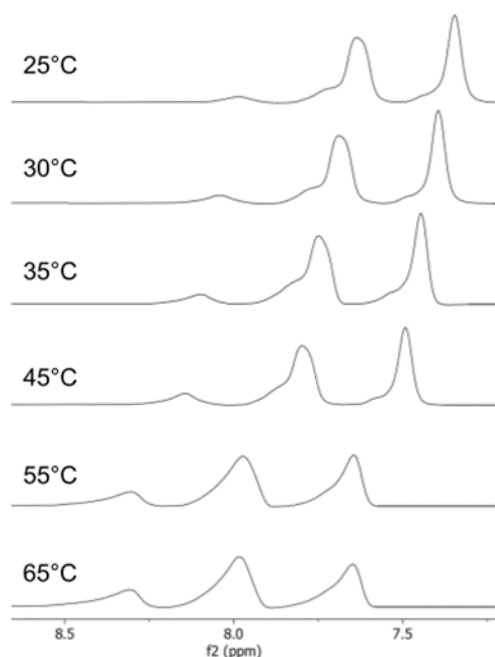


Figure S3: 1D ¹H NMR spectra of a variable temperature experiment performed on a single sample of 44 mM MK-2 incorporated into 130 mM EPC liposomes. Significant coalescence of aqueous and liposomal aromatic peaks was not observed, indicating that any exchange between the aqueous and liposomal populations is occurring on a different timescale.